Quaternary Science Reviews
February 2020, Volume 229 Pages 106134 (16p.)
https://doi.org/10.1016/j.quascirev.2019.106134
https://archimer.ifremer.fr/doc/00598/71058/

Analysing the timing of peak warming and minimum winter sea-ice extent in the Southern Ocean during MIS 5e

Chadwick M. [1, 2, *], Allen C.S. [1], Sime L.C. [1], Hillenbrand C.-D. [1]

[1] British Antarctic Survey, High Cross, Madingley Road, Cambridge, CB3 0ET, UK
[2] Ocean and Earth Science, National Oceanography Centre, University of Southampton Waterfront Campus, European Way, Southampton, SO14 3ZH, UK

* Corresponding author : M. Chadwick, email address : machad27@bas.ac.uk

Abstract :

The peak of the Last Interglacial, Marine Isotope Stage (MIS) 5e (130e116 ka), provides a valuable 'process analogue' for validating the climatic feedbacks and forcings likely active under future anthropogenic warming. Reconstructing exact timings of MIS 5e peak warming and minimum winter sea-ice extent (WSIE) throughout the Southern Ocean (SO) will help to identify the interactions and feedbacks within the ice-ocean system. Here we present a new MIS 5e marine sediment record from the SWAtlantic sector together with 28 published core records (chronologies standardised to the LR04 d18O benthic stack; Lisiecki and Raymo, 2005) to investigate the timing and sequence of minimum WSIE and peak warming across the SO. Sea-surface temperatures (SSTs) peaked earliest in the Indian (20oEe150oE) and Atlantic (70oWe20oE) sectors, at 128.7 ± 0.8 ka and 127.4 ± 1.1 ka respectively, followed by the Pacific sector (150oEe70oW) at 124.9 ± 3.6 ka. The interval of minimum WSIE for all three sectors occurred within the period from 129e125 ka, consistent with the ~128 ka sea salt flux minimum in Antarctic ice cores. Minimum WSIE appears to have coincided with peak July insolation at 55 oS, suggesting it could be linked with the mildest winters. The reduced WSIE during MIS 5e would have likely reduced the production of deep- and bottom water masses, inhibiting storage of CO2 in the abyssal ocean and lowering nutrient availability in SO surface waters. Examining a wide spatial range of proxy records for MIS 5e is a critical step forward in understanding climatic interactions and processes that will be active under warmer global temperatures.

Highlights

► MIS 5e peak sea-surface temperatures occur synchronously in the Indian and Atlantic sectors. ► The Pacific sector reaches maximum sea-surface temperatures later than the Indian and Atlantic sectors during MIS 5e. ► MIS 5e minimum winter sea ice extent occurs synchronously throughout the Southern Ocean

.

Keywords : Interglacial, Sediment cores, Palaeoceanography, Southern Ocean

1. Introduction

The Antarctic region has a critical role in the climate system. Strong climate feedbacks arise because of albedo changes due to the vast extent of the Antarctic ice sheet and sea ice across the Southern Ocean (SO). In addition to the albedo-radiation feedbacks, sea ice cover also regulates heat and gas exchange between the atmosphere and the ocean as well as changes in sea surface temperature (SST), sea ice formation rate, and salinity that affect deep water mass production and, thus, impact on global ocean circulation. Therefore, the high latitudes are particularly important for a better understanding of the climate system due to their greater sensitivity to radiative forcing and their ability to amplify the effects of rising temperatures, particularly through oceanic and cryosphere feedbacks (Vaughan et al. 2013).

At present, rising greenhouse gas concentrations are driving global warming, with polar regions warming faster than other regions, largely due to albedo feedbacks (IPCC 2018). Studying past warm periods, when ice sheet and sea-ice extents were reduced, may help us better understand the impacts of future climate changes in these key regions.

The last period which was substantially warmer in the southern polar region was the last interglacial. The peak of this last interglacial period, centred at 128-126 ka, occurred during Marine Isotope Stage (MIS) 5e (130 – 116 ka). It was characterised by naturally forced global mean annual atmospheric and sea-surface temperatures (SSTs), which were 1.0-1.5 ^{o}C warmer than present (Masson-Delmotte et al. 2011, Capron et al. 2014), with global sea level 5-9m higher than today (Kopp et al. 2009). Mean annual SSTs in middle and low latitudes during this MIS 5e peak were probably just 0.5 ± 0.3 ^{o}C warmer than

pre-industrial (Holloway et al. 2017) and thus imply polar amplification, with model results indicating that summer SSTs in the SO were 1.8 ± 0.8 °C higher than preindustrial (Capron et al. 2017). SSTs in the SO are estimated to have increased by ca. 3-6 °C during the penultimate glacial-interglacial transition (Bianchi & Gersonde 2002, Hayes et al. 2014). MIS 5e with its peak is not a true analogue for future anthropogenic warming, as it was orbitally forced rather than through increased greenhouse gas concentrations. Nevertheless, understanding the natural responses and feedbacks that characterise MIS 5e climate will provide valuable insight into the mechanisms that will be active in a future warmer climate (Stone et al. 2016), making MIS 5e an important 'process analogue'.

Understanding the timing of Antarctic warming and changes in SO sea-ice extent during MIS 5e is crucial when attempting to determine which feedbacks and processes are dominant (e.g. Antarctic summer insolation, strength of North Atlantic downwelling, changes to the West Antarctic Ice Sheet), and thereby improve the accuracy of predictions. Heterogeneity in SO sea ice trends has been observed over the last four decades, when a reduction in the Bellingshausen and Amundsen seas was concurrent with an increase in the Weddell Sea, the Ross Sea and in the Indian and western Pacific sectors of the SO (Stammerjohn et al. 2008, King 2014, Parkinson 2019). Modern surface, deep and bottom-water temperature trends display a similar spatial heterogeneity throughout the SO (Maheshwari et al. 2013, Schmidtko et al. 2014), indicative of the complexity of the climate system and the mechanisms driving SST and sea ice change in the present day (Stammerjohn et al. 2008, Hobbs et al. 2016, Purich et al. 2016). There is also temporal heterogeneity in the SO sea ice trends (Parkinson 2019), with the Amundsen sea region showing a large decrease in summer sea ice concentration but a coinciding increase in winter sea ice concentration (Hobbs et al. 2016).

Several previous studies have combined model simulations of the climate during MIS 5e with proxy records from Antarctic ice cores and with – or without – the limited data constraints available from marine sediment cores recovered predominantly in the Sub-Antarctic (Otto-Bliesner et al. 2013, Bakker et al. 2014, Capron et al. 2014, Holloway et al. 2016, Stone et al. 2016, Capron et al. 2017,

74 Holloway et al. 2017). However, due to the uncertainties in the chronologies of proxy records (Govin
75 et al. 2015), these comparisons assume synchronous peak surface water warming in the SO and peak
76 atmospheric warming in Antarctica (Otto-Bliesner et al. 2013, Capron et al. 2014, Capron et al. 2017).
77 The sea ice minimum is also assumed to be synchronous across the SO, with Holloway et al. (2017)
78 modelling it to occur at 128 ka, i.e. coeval with the peak Antarctic atmospheric temperature recorded
79 in ice cores. The high spatial and temporal heterogeneity for both sea ice and SST trends in the modern
80 SO highlights the need to examine with care this assumed synchronicity.

81 This paper aims to establish whether the timing of peak SSTs, and the winter sea ice minimum
82 (hereafter simply referred to as the "sea ice minimum"), occurs synchronously throughout the SO
83 during MIS 5e. We do this by compiling published data from marine sediment records distributed
84 between 40 ^{o}S and 65 ^{o}S. This compilation looks at synchronicity both across the SO and within its
85 Atlantic (70^{o}W–20^{o}E), Indian (20^{o}E–150^{o}E) and Pacific sectors (150^{o}E–70^{o}W). Published sea ice data
86 from the three sectors are compared with a new sea ice record (core TPC288). The ages for the sea
87 ice minimum are compared between cores and referenced to the ages for peak SSTs in the published
88 records. SSTs can also be used as a basis to reconstruct the positions of the main SO fronts during the
89 period of peak MIS 5e warmth. However, these frontal reconstructions are limited by the variations
90 in the latitudinal position of a front across a sector (Moore et al. 1999, Sokolov & Rintoul 2009),
91 particularly in areas, where fronts are 'pinned' by bathymetric constraints, such as in parts of the
92 Scotia Sea (Moore et al. 1999), and thus their positions are less able to shift.

93 Specifically, we aim to determine whether:

94 - Peak SSTs for MIS 5e occur at the same time in each SO sector and coincide with the peak
95 warming in Antarctic ice cores.
96 - Peak SSTs are coincident with the minimum winter sea-ice extent (WSIE).
97 - An increase in southern hemisphere July insolation accounts for the SST warming and
98 reduction in WSIE.

2. Modern Oceanography

The modern oceanography of the SO is dominated by the clockwise flowing Antarctic Circumpolar Current (ACC) which forms a band of high geostrophic shear around Antarctica (Orsi et al. 1995). The ACC is characterised by five major fronts which represent changes in the water density due to varying temperatures and salinities (Orsi et al. 1995, Moore et al. 1999, Dong et al. 2006, Sokolov & Rintoul 2009). The two most southerly fronts, the southern boundary of the ACC and the Southern ACC Front, do not mark the boundary between distinct surface water masses and will not be considered as part of this review. The most northerly of the remaining fronts is the Subtropical Front (STF) that marks the northern boundary of both the ACC and Subantarctic surface waters. The STF is marked by surface water temperature changes of 4-5 ^{o}C across the front with waters to its north generally being warmer than 14 ^{o}C (Sikes et al. 2002). The modern STF is located at around 41 ^{o}S in the Atlantic and Indian sectors of the SO and on average at 39 ^{o}S in the Pacific sector (Figure 1). To the south of the STF is the Subantarctic Front (SAF) which is marked by SSTs greater than ~ 6-8 ^{o}C (Meinen et al. 2003). The SAF is currently located at an average latitude of 45 ^{o}S, 48 ^{o}S and 57 ^{o}S in the Atlantic, Indian and Pacific sectors, respectively (Figure 1). The most southerly of the three main ACC fronts is the Polar Front (PF) which, in general corresponds to SSTs of ~ 2-3 ^{o}C (Dong et al. 2006) and which is currently located at around 50 ^{o}S in the Atlantic sector, 55 ^{o}S at 100 ^{o}E in the Indian sector and 60 ^{o}S at 170 ^{o}W in the Pacific sector (Figure 1). The region south of the PF (and north of the southern ACC Front) is called the Antarctic Zone, the region between the PF and the SAF is the Polar Frontal Zone, and the region between the SAF and STF is the Subantarctic Zone (Orsi et al. 1995). In the modern ocean the position of fronts is determined using various methods, such as longitudinal SST gradients (Moore et al. 1999, Dong et al. 2006), hydrographic sections (Orsi et al. 1995, Belkin & Gordon 1996), sea surface heights (Sokolov & Rintoul 2009) or a combination of methods, with the sea-surface height approach showing the splitting and recombining of frontal 'filaments' in areas without bathymetric 'pinning' (Sokolov & Rintoul 2009). Because these various methods were used in the previous studies at different times to identify frontal positions (Orsi et al. 1995, Belkin & Gordon 1996, Moore et al. 1999, Dong et al. 2006,

125 Sokolov & Rintoul 2009), the frontal positions are not fully consistent as different 'filaments' may have
126 been mapped.

127 ## 3. Core sites

128 This study presents 32 published records from 28 sediment cores across the SO (Figure 1) with 17
129 records providing ages for MIS 5e peak summer SST and 15 records providing ages for peak annual
130 SST (Table 1). All SO cores south of 40 °S, for which a chronology and SST record had been published,
131 are included, with some records having been included in multiple previous publications, e.g. when
132 various SST proxies were analysed on the same core, such as for ODP Leg 177 Site 1094 (Bianchi &
133 Gersonde 2002, Hayes et al. 2014). For each site, the MIS 5e summer and annual SSTs (hereafter jointly
134 referred to as SSTs c.f. Waelbroeck et al. (2009)) are compared with corresponding modern SSTs so
135 that MIS 5e SST anomalies are standardised across all records. There are 11 published MIS 5e sea ice
136 records from 10 sediment cores in addition to the new record from site TPC288 in the Scotia Sea, for
137 which no SSTs are available. Eleven of the 29 core sites are located in the Atlantic sector, 7 in the
138 Indian sector and 11 in the Pacific sector. The methods for reconstructing past SSTs and establishing
139 age models vary between cores (Table 1) but the sea ice minimum consistently utilises the Gersonde
140 & Zielinski (2000) proxy for the presence of the WSIE. Accordingly, the age of the MIS 5e sea ice
141 minimum is reported here as the interval when the combined abundance percentages of the sea-ice
142 diatom species *Fragilariopsis curta* + *Fragilariopsis cylindrus* (FCC) reached its minimum (Gersonde &
143 Zielinski 2000). FCC abundances >3 % indicate a site located at and south of the mean WSIE (edge of
144 the mean WSIE ~ 50-80 % concentration in September for 1982 to 2002) (Gersonde et al. 2005). FCC
145 abundances between 1 and 3 % indicate the position of a site south of the limit of maximum WSIE
146 (mean concentration ~ 15-20 %) and north of the mean WSIE, whereas abundances <1 % indicate a
147 site position north of the maximum WSIE (Gersonde et al. 2003, Gersonde et al. 2005). Several of the
148 cores also have published transfer function estimates of MIS 5e sea ice, but for consistent comparison
149 only the FCC records are considered in this study. Table 1 contains the details for each of the studied

150

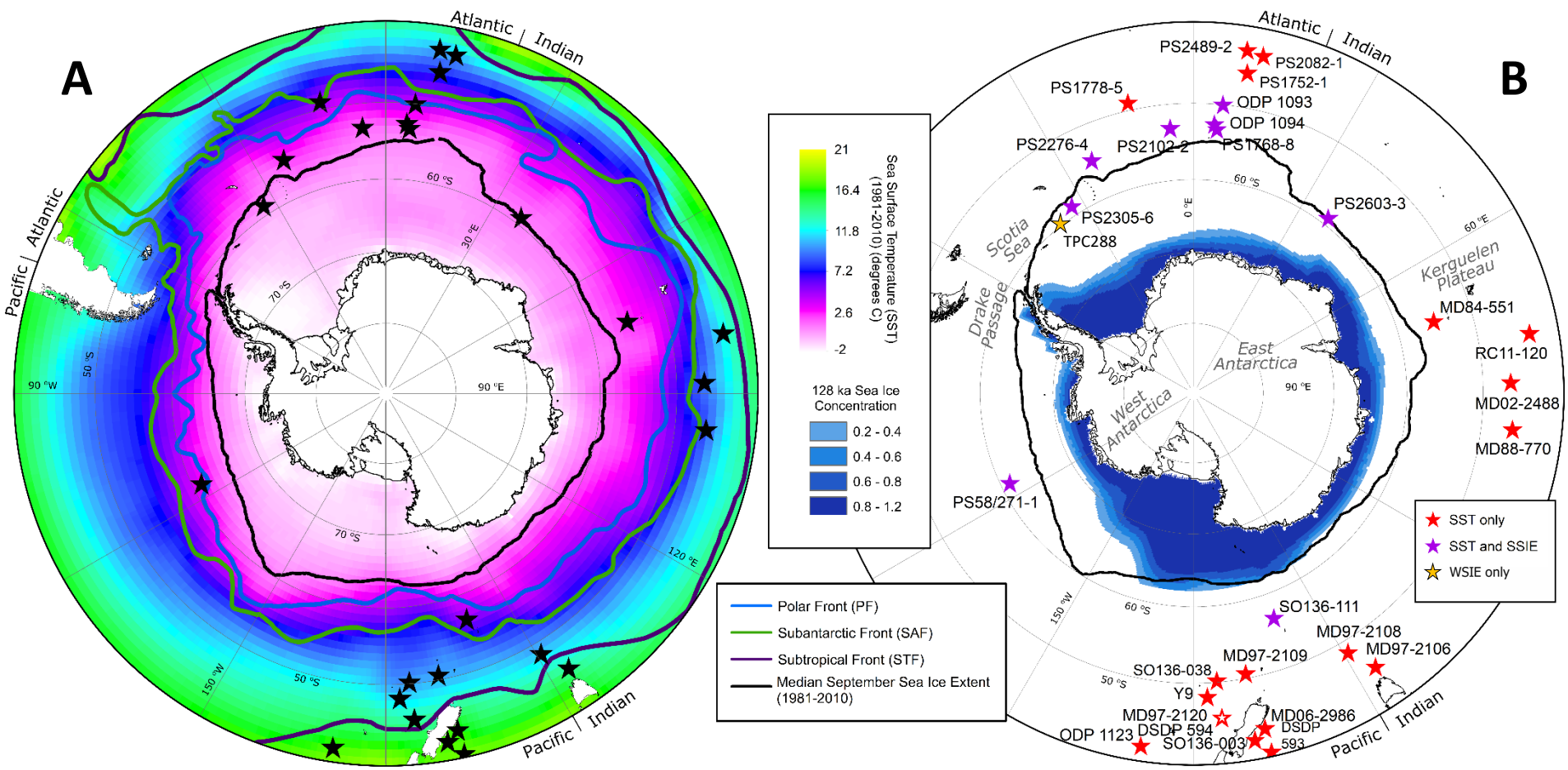

Figure 1: A - Map of modern (1981-2010) mean Sea Surface Temperatures (SST) and average September sea-ice extent with Antarctic frontal positions. Black stars mark the positions of published core records used in this study. **B** - Map comparing modern average September sea-ice extent with modelled September sea ice concentrations for 128 ka (Holloway et al. 2017). The core sites marked by red stars have published SSTs only, the sites marked by purple stars have published SSTs and sea ice records. The orange star marks the location of the new MIS 5e sea ice record from site TPC288 in the Scotia Sea. The red star with white centre marks the position of neighbouring core sites MD97-2120 and DSDP Site 594. Both maps show the region south of 40 °S. The positions of the Subtropical Front (STF) and Subantarctic Front (SAF) are from Orsi et al. (1995) and that of the Polar Front (PF) is from Trathan et al. (2000).

Core	Latitude (°S), Longitude (°E)	Oceanographic Position	Modern SST (°C) (*summer SST)	Modern Sea Ice	Chronology for MIS 5e	SST Proxy for MIS 5e	Sample Resolution (ka)
Atlantic sector							
PS2489-2	42.87, 8.97	SAZ	10* (Becquey & Gersonde 2003)	1	SPECMAP ages (Becquey & Gersonde 2003) converted onto LR04 (this study)	Planktonic foraminifera transfer function (Becquey & Gersonde 2003)	1.2-3
PS2082-1	43.22, 11.74	SAZ	11.08* (Waelbroeck et al. 2009)	1	SPECMAP ages (Brathauer & Abelmann 1999) converted onto LR04 (this study)	Radiolarian transfer function (Brathauer 1996)	5
PS1752-1	45.62, 9.60	SAZ	8.00* (Brathauer 1996)	1	*C. davisiana* stratigraphy (Brathauer 1996) converted onto LR04 (this study)	Radiolarian transfer function (Brathauer 1996)	10-22
PS1778-5	49.01, -12.7	PFZ	4.38* (Waelbroeck et al. 2009)	1	SPECMAP ages (Brathauer & Abelmann 1999) converted onto LR04 (this study)	Radiolarian transfer function (Brathauer & Abelmann 1999)	1.2-5
ODP 1093	49.98, 5.87	AZ	3.6* (Schneider Mor et al. 2012)	1	EDC3 ages (Schneider Mor et al. 2012) converted onto LR04 (this study)	Diatom transfer function (Schneider Mor et al. 2012)	1
PS1768-8	52.59, 4.48	AZ	2.5* (Waelbroeck et al. 2009)	1	Correlating planktonic (*N. pachyderma*$_{(sin)}$) $\delta^{18}O$ (Mulitza et al. 1999) with LR04 (this study)	Diatom transfer function (Zielinski et al. 1998)	1-4
PS2102-2	53.07, -4.99	AZ	1.84* (Waelbroeck et al. 2009)	1	Correlating planktonic (*N. pachyderma*$_{(sin)}$) $\delta^{18}O$ (Niebler 1995) with LR04 (this study)	Diatom transfer function (Bianchi & Gersonde 2002)	0.6-3
ODP 1094	53.18, 5.13	AZ	2.2* (Capron et al. 2014)	1	EDC3 ages (Schneider Mor et al. 2012) converted onto LR04 (this study) Correlating planktonic (*N. pachyderma*$_{(sin)}$) $\delta^{18}O$ (Kanfoush et al. 2002) with LR04 (this study)	Diatom transfer function (Bianchi & Gersonde 2002, Schneider Mor et al. 2012)	0.07-1.4 1
PS2276-4	54.64, -23.57	AZ	1.71* (Waelbroeck et al. 2009)	2	Diatom biofluctuation zones (Bianchi & Gersonde 2002)	Diatom transfer function (Bianchi & Gersonde 2002)	0.8-1.6
PS2305-6	58.72, -33.04	AZ	0.78* (Waelbroeck et al. 2009)	3	Diatom biofluctuation zones (Bianchi & Gersonde 2002)	Diatom transfer function (Bianchi & Gersonde 2002)	0.5-4.1
TPC288	59.14, -37.96	AZ	1.5* (Allen 2014)	3	EDC3 ages (Pugh et al. 2009) converted onto LR04 (this study)	-	1.1

Core	Latitude (°S), Longitude (°E)	Oceanographic Position	Modern SST (°C) (*summer SST)	Modern Sea Ice	Chronology for MIS 5e	SST Proxy for MIS 5e	Sample Resolution (ka)
Indian sector							
RC11-120	43.52, 79.87	SAZ	11.43* (Waelbroeck et al. 2009)	1	SPECMAP ages (Martinson et al. 1987) converted onto LR04 (this study)	Radiolarian transfer function (Hays et al. 1976)	1.3-2.5
MD97-2106	45.15, 146.29	N of STF	12.58 (Cortese et al. 2013)	1	Correlating benthic $\delta^{18}O$ with LR04 (Cortese et al. 2013)	Planktonic foraminifera transfer function (Cortese et al. 2013)	1.2-1.6
MD88-770	46.02, 96.45	SAZ	8.1* (Govin et al. 2009)	1	Correlating benthic (*C. wuellerstorfi, M. barleeanum & E. exigua*) $\delta^{18}O$ (Labeyrie et al. 1996) with LR04 (this study)	Planktonic foraminifera transfer function (Barrows et al. 2007)	0.1-0.5
MD02-2488	46.48, 88.02	SAZ	9.1* (Govin et al. 2009)	1	Correlating benthic (*C. kullenbergi*) $\delta^{18}O$ (Govin et al. 2009) with LR04 (this study)	Planktonic foraminifera transfer function (Govin et al. 2009)	1-2
MD97-2108	48.5, 149.11	SAZ	9.49 (Cortese et al. 2013)	1	Correlating benthic $\delta^{18}O$ with LR04 (Cortese et al. 2013)	Planktonic foraminifera transfer function (Cortese et al. 2013)	2.8-2.9
MD84-551	55, 73.33	AZ	2.49* (Waelbroeck et al. 2009)	1	Correlating planktonic (*N. pachyderma*$_{(sin)}$) $\delta^{18}O$ (Pichon et al. 1992) with LR04 (this study)	Diatom transfer function (Pichon et al. 1992)	0.27-0.66
PS2603-3	58.99. 37.63	AZ	1.82* (Waelbroeck et al. 2009)	2	Diatom biofluctuation zones (Bianchi & Gersonde 2002)	Diatom transfer function (Bianchi & Gersonde 2002)	0.9-1.9
Pacific sector							
DSDP 593	40.51, 167.67	N of STF	15.61 (Cortese et al. 2013)	1	Correlating benthic $\delta^{18}O$ with LR04 (Cortese et al. 2013)	Planktonic foraminifera transfer function (Cortese et al. 2013)	3.2-9.7
ODP 1123	41.79, -171.5	N of STF	14.94 (Cortese et al. 2013)	1	Correlating benthic $\delta^{18}O$ with LR04 (Cortese et al. 2013)	Planktonic foraminifera transfer function (Cortese et al. 2013)	2.4-3.1
SO136-003	42.3, 169.88	N of STF	15.4 (Pelejero et al. 2006) 15.55 (Cortese et al. 2013)	1	Converting SPECMAP ages (Pelejero et al. 2006) onto LR04 (this study) Correlating planktonic (*G. bulloides*) $\delta^{18}O$ (Barrows et al. 2007) with LR04 (this study) Correlating benthic $\delta^{18}O$ with LR04 (Cortese et al. 2013)	Alkenone based $U^{K'}_{37}$ (Pelejero et al. 2006) Planktonic foraminiferal transfer functions (Barrows et al. 2007) Planktonic foraminifera transfer function (Cortese et al. 2013)	0.5-3 0.5-4 0.8-4.4
MD06-2986	43.45, 167.9	N of STF	14.93 (Cortese et al. 2013)	1	Correlating benthic $\delta^{18}O$ with LR04 (Cortese et al. 2013)	Planktonic foraminifera transfer function (Cortese et al. 2013)	1.8-3.9

Core	Latitude (°S), Longitude (°E)	Oceanographic Position	Modern SST (°C) (*summer SST)	Modern Sea Ice	Chronology for MIS 5e	SST Proxy for MIS 5e	Sample Resolution (ka)
DSDP 594	45.52, 174.95	SAZ	10.41 (Cortese et al. 2013)	1	Correlating benthic $\delta^{18}O$ with LR04 (Cortese et al. 2013) Correlating benthic (*Uvigerina* sp.) $\delta^{18}O$ (Nelson et al. 1993) with LR04 (this study)	Planktonic foraminifera transfer function (Cortese et al. 2013) Planktonic foraminifera transfer functions (Barrows et al. 2007)	0.1-2.1 0.5-16
MD97-2120	45.54, 174.93	SAZ	11.8 (Pahnke et al. 2003)	1	Correlating planktonic (*G. bulloides*) $\delta^{18}O$ (Pahnke et al. 2003) to LR04 (this study)	Mg/Ca composition of *Gg. bulloides* (Pahnke et al. 2003)	0.5-1
Y9	48.24, 177.34	SAZ	8.82 (Cortese et al. 2013)	1	Correlating benthic $\delta^{18}O$ with LR04 (Cortese et al. 2013)	Planktonic foraminifera transfer function (Cortese et al. 2013)	1.9-2.7
SO136-038	50.22, 175.31	SAZ	8.00 (Cortese et al. 2013)	1	Correlating benthic $\delta^{18}O$ with LR04 (Cortese et al. 2013)	Planktonic foraminifera transfer function (Cortese et al. 2013)	5.6-5.7
MD97-2109	50.63, 169.38	SAZ	9.05 (Cortese et al. 2013)	1	Correlating benthic $\delta^{18}O$ with LR04 (Cortese et al. 2013)	Planktonic foraminifera transfer function (Cortese et al. 2013)	1.9-2.9
SO136-111	56.67, 160.23	PFZ	5.54* (Waelbroeck et al. 2009)	1	SPECMAP ages (Crosta et al. 2004) converted onto LR04 (this study)	Diatom transfer function (Crosta et al. 2004)	0.5-1.7
PS58/271-1	61.24, -116.05	PFZ	3.05* (Waelbroeck et al. 2009)	1	EDC3 ages (Benz et al. 2016) converted onto LR04 (this study)	Diatom transfer function (Esper & Gersonde 2014b)	0.1-0.2

151

Table 1: Details for the cores analysed as part of this study. Cores are ordered by latitude within the three SO sectors (Atlantic-Indian-Pacific). The position of the cores relative to the modern SO fronts is given along with the modern SST (asterisks indicate summer SST rather than mean annual SST) and the present sea ice conditions. For the sea ice conditions (cf. Gersonde et al. 2003, Gersonde et al. 2005): 1 – core is located north of the maximum winter sea ice limit (FCC <1 %), 2 – core is located north of the mean and south of the maximum winter sea ice limit (FCC =1-3 %), 3 – core is located at or south of the mean winter sea ice limit (FCC >3 %) (limit of maximum sea-ice extent is based on ~15-20 % concentration for September (winter) and February (summer) for the years 1982 to 2002). The chronological method applied to a core and the proxy method used to determine MIS 5e SSTs together with the sample resolution and the source data references are also given. AZ: Antarctic Zone, PFZ: Polar Frontal Zone, SAZ: Subantarctic Zone, STF: Subtropical Front.

cores, with geographical location, modern SST, sea ice concentration, and core location in respect to frontal positions, as well as the methodological details for the age models and proxies used for the MIS 5e SST reconstructions, including the data source references. Sample resolution for the interval spanning MIS 5e is also given.

4. Age models

An important consideration for the published records is the robustness of their age models and the comparability between records. The publications of the records span nearly 30 years and thus use a range of chronologies (details in Supplementary Table 1). In order to improve the robustness of our comparison we calibrated the age models of the records, where possible, to the LR04 benthic foraminifera $\delta^{18}O$ stack (Lisiecki & Raymo 2005). The majority of the 33 core records were either originally published on the LR04 scale (10 records) or could be converted from the SPECMAP age scale (6 records) or from the EDC3 time-scale for the EPICA Dome C ice core in East Antarctica (4 records) (Table 1). Records published on the SPECMAP and EDC3 age scales were translated onto the LR04 chronology using the conversion tables from Lisiecki & Raymo (2005) and Parrenin et al. (2013), respectively. Nine of the records (DSDP 594, MD88-770, MD02-2488, MD84-551, ODP site 1094, SO136-003, PS1768-8, PS2102-2 and MD97-2120) were converted to the LR04 scale by tying the $\delta^{18}O$ data for each core to the LR04 stack (Figure 2, Supplementary Figures 1 & 2) using the Analyseries software (Paillard et al. 1996). For three of these records benthic $\delta^{18}O$ data (Supplementary Figure 1) and for the other six planktonic $\delta^{18}O$ data were available (Figure 2, Supplementary Figure 2). For the correlation of $\delta^{18}O$ curves we selected tie-points (Supplementary Table 3) (Chadwick 2019a) that marked the midpoint of major $\delta^{18}O$ shifts at MIS stage or sub-stage boundaries (for details, see Supplementary materials).

For all the records on the LR04 time scale the stated error during the last 1 Ma is ~ 4 ka (Lisiecki & Raymo 2005). However, for distinct shifts in the LR04 stack (e.g. Termination II) the error on the chronology is likely to be <3 ka (Cortese et al. 2013). The most robust age models are from cores with

benthic foraminifera $\delta^{18}O$ data that could be directly correlated with the LR04 stack, and cores with existing SPECMAP or EDC3 tuned chronologies could be translated onto the LR04. Age models based on correlations of planktonic foraminifera $\delta^{18}O$ data obtained from the corresponding cores with the LR04 stack are considered less robust because changes in surface water temperatures incorporated in the $\delta^{18}O$ signals of planktonic foraminifera are unlikely to be fully synchronous with the changes in deep water $\delta^{18}O$ composition (mainly global ice volume) represented by the benthic LR04 stack. The

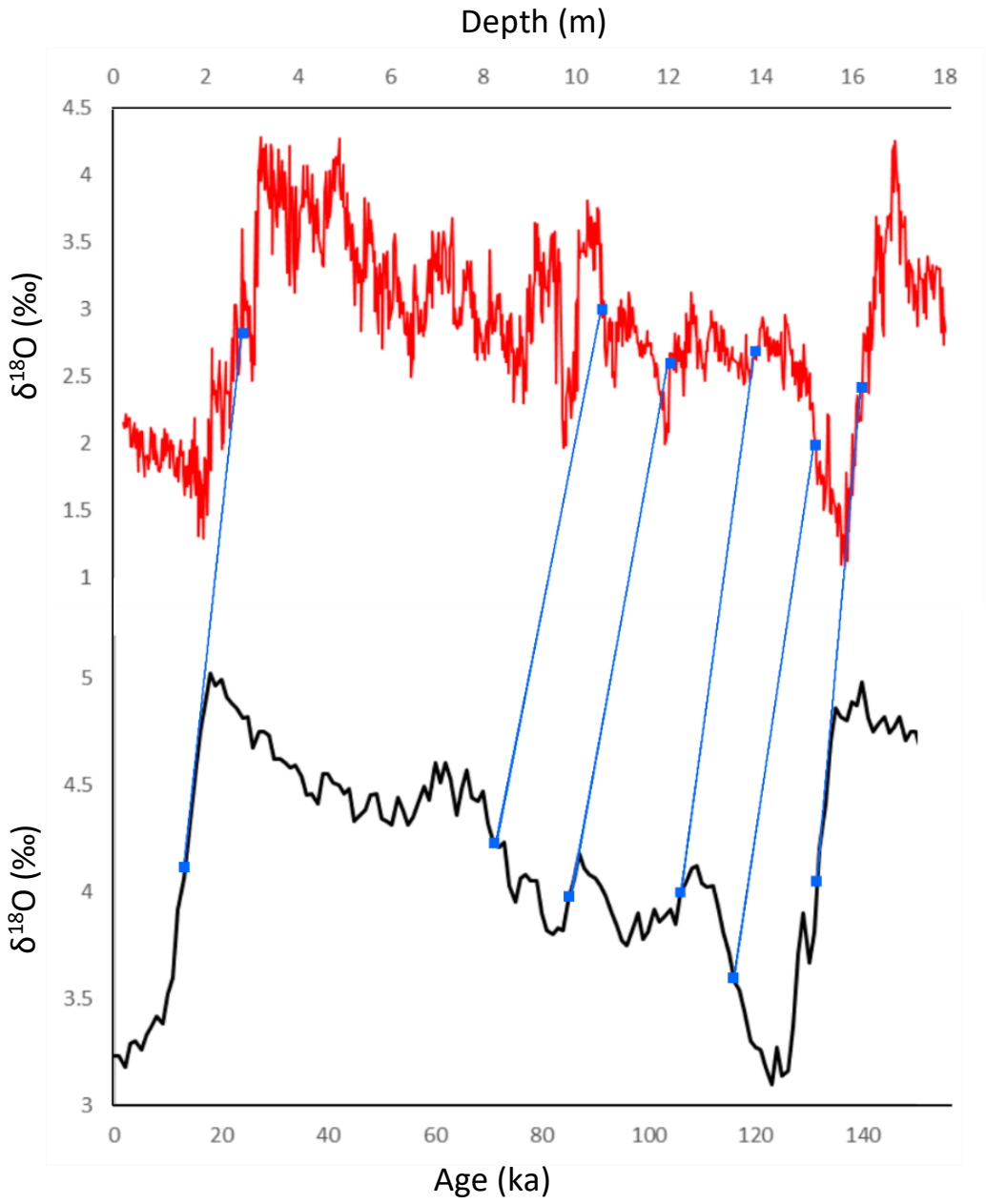

Figure 2: Example of correlation between planktonic foraminifera $\delta^{18}O$ data (red) from a core (here: MD97-2120) and the LR04 stack (black) using Analyseries software. Tiepoints are marked by blue squares and connecting lines, with age assignments for MIS 5 sub-stages following Govin et al. (2009).

least robust chronologies are those for the four records without $\delta^{18}O$ data, which were dated by diatom biofluctuation stratigraphy (PS2276-4, PS2603-3 and PS2305-6) (Bianchi & Gersonde 2002) or *Cycladophora davisiana* radiolarian abundance stratigraphy (PS1752-1) (Brathauer et al. 2001). The stratigraphy for core PS1752-1 was converted onto the LR04 scale using the *C. davisiana* peak ages published by Pugh et al. (2009).

For cores with age models of different robustness (e.g. ODP Site 1094 and SO136-003), the ages for peak SSTs are within 2 ka and therefore within the error of the LR04 stack. Similarly, for the three cores with the least robust age models the ages of peak warming are within 1-2 ka of other Atlantic and Indian sector records situated south of the PF. The consistency between ages for MIS 5e SST peaks in records with different age model robustness but from the same SO sector justifies the inclusion of all records in the analysis of the timing of MIS 5e peak SSTs and sea ice minima in the different SO sectors. All cores, for which SSTs had been correlated to ice core deuterium records (ODP Site 1094, MD02-2488, MD97-2120; Supplementary Table 1), were tied to the LR04 stack using their benthic (MD02-2488) or planktonic (ODP Site 1094 and MD97-2120) $\delta^{18}O$ records to allow an independent comparison between the SST record from the sediment cores and the atmospheric temperature record from Antarctic ice cores. Hereafter all ages refer to the LR04 stack unless otherwise stated.

5. Materials and methods for TPC288

Core TPC288 (Lat. 59.14 ^{o}S, Lon. 37.97 ^{o}W; water depth 2864m) was recovered in the Scotia Sea during cruise JR48 with RRS *James Clark Ross* in 2000. Trigger core TC288 and piston core PC288 were spliced to produce a continuous core record with a composite length of 940 cm. Microscope slides for the study of diatom assemblages were produced using a method adapted from Scherer (1994) at a depth resolution of 2 cm for the MIS 5e core interval, which spans the depth from 398 to 416 cm. Samples of 8-15mg were exposed to 10% Hydrochloric acid to remove any carbonate and 30% Hydrogen Peroxide to break down the organic material. A 4% Sodium Hexametaphosphate solution was added to the solution for disaggregation, and the material was then allowed to settle randomly onto

coverslips over a minimum of 4 hours. Slides were investigated with a light microscope (Olympus BH-2 at x1000 magnification), and a minimum of 300 diatom valves were counted for each sample. The FCC value for each sample was calculated as a percentage of the total diatom assemblage. The previously published age model for core TPC288 is based on the correlation of its magnetic susceptibility record with dust concentration in the EPICA Dome C ice core and constrained by *C. davisiana* stratigraphy (Pugh et al. 2009).

6. Results

The MIS 5e SST and WSIE records, including ages for the maximum SSTs and the associated errors from the sample resolution, are compiled in Table 2. Even though it was possible to determine an age relationship between the MIS 5e SST maximum and WSIE minimum in all three SO sectors, the exact age of the MIS 5e sea ice minimum at a particular core site could often not be precisely constrained as almost all records have extended MIS 5e sediment intervals, in which specimens of *F. curta* and *F. cylindrus* are absent (FCC = 0). Exceptions are the MIS 5e records from core sites PS2305-6 and TPC288, where the percentages of both taxa during the WSIE minimum never fall below 0.8% and 0.3%, respectively. However, all sites have in common a prolonged MIS 5e period when the site was located north of the mean WSIE (FCC =1-3%), and at least a short MIS 5e episode when the site was located north of the maximum WSIE (FCC <1%) (cf. Bianchi & Gersonde 2002).

6.1. Sea Surface Temperatures

The average ages of peak SSTs during MIS 5e range from 128 ka to 125 ka and thus lie within 3 ka throughout the three SO sectors, with the full range of ages spanning 129-123 ka (Table 2 & Figure 3). The SST maxima in the Atlantic and Indian sectors are both well constrained and occurred on average at 127.4 ± 1.1 ka and 128.7 ± 0.8 ka, respectively (errors are one standard deviation). In contrast, peak MIS 5e SSTs in the Pacific sector show with an average age of 124.9 ± 3.6 ka, a much larger range.

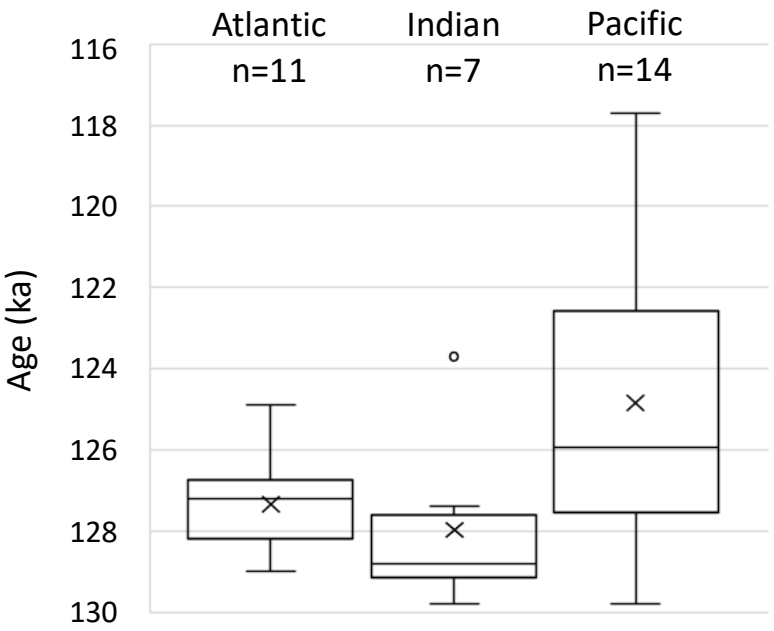

Figure 3: Box plots showing the age distribution of peak SSTs in the three SO sectors during MIS 5e. A × marks the mean age for each sector. The horizontal line within each box marks the median; the box demarcates the interquartile range and the extended vertical lines illustrate the full age range of peak SSTs in each sector. The circle marks an anomalous age from core MD88-770.

231 During MIS 5e SSTs shifted southwards in the SO (Brathauer & Abelmann 1999, Benz et al. 2016).
232 Assuming that the isotherms delineating the modern ACC fronts did so during MIS 5e, too (Bianchi &
233 Gersonde 2002), we used the MIS 5e peak SST from each core to assign its oceanographic zone during
234 that time (Table 2; see section 6.3. below). Cores located in the Subantarctic Zone reveal a later
235 average age of MIS 5e peak SSTs, i.e. at 124.1 ± 3.6 ka, than those north of the STF and in the Polar

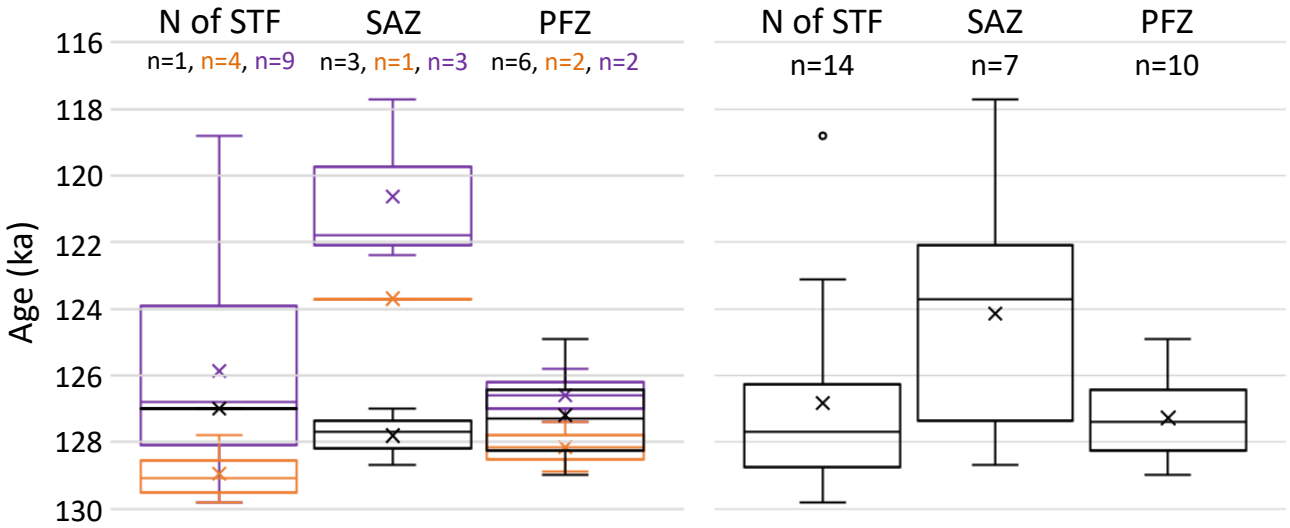

Figure 4: Box plots showing the age distribution of peak SSTs in the oceanographic zones of each sector (**LHS**) and the entire SO (**RHS**) during MIS 5e (STF: Subtropical Front; PFZ: Polar Frontal Zone, SAZ: Subantarctic Zone). Black – Atlantic, Orange – Indian, Purple – Pacific. There is only one MIS 5e Antarctic Zone record (PS2305-6) which has peak SSTs at 127 ± 0.7 ka. × marks the mean age for each sector. The horizontal line within each box marks the median; the box demarcates the interquartile range and the extended vertical lines illustrate the full range of values.

	Age of MIS 5e Sea Ice Min (ka)	MIS 5e Minimum Sea Ice Conditions	Age of MIS 5e SST peak (ka)	Error on MIS 5e SST peak age (ka)	MIS 5e Peak SST (°C) (*summer SST)	MIS 5e oceanographic zone	References for MIS 5e Conditions
Atlantic sector							
PS2489-2	-	-	127.7	±0.8	11.8*	SAZ	(Becquey & Gersonde 2003)
PS2082-1	-	-	127.0	±2.5	14.1*	N of STF	(Brathauer & Abelmann 1999)
PS1752-1	-	-	128.7	+10.9,-4.9	6.0*	SAZ	(Brathauer 1996)
PS1778-5	128.2 ± 1.3	1	127.0	+2.4, -0.6	6.8*	SAZ	(Brathauer & Abelmann 1999, Gersonde & Zielinski 2000)
ODP 1093	125.0 ± 1.2	1	124.9	±0.3	5.0*	PFZ	(Schneider Mor et al. 2012)
PS1768-8	127.5 ± 1.3	1	128.1	±1.0	3.9*	PFZ	(Zielinski et al. 1998)
PS2102-2	127.1 ± 3.2	1	129.0	±0.6	3.8*	PFZ	(Bianchi & Gersonde 2002)
ODP 1094	126.9 ± 4.1 125.8 ± 1.6	1 1	128.3 126.4	±0.1 ±0.1	4.7* 4.8*	PFZ PFZ	(Bianchi & Gersonde 2002) (Schneider Mor et al. 2012)
PS2276-4	128.2 ± 0.5	1	126.5	+0.5,-0.4	3.1*	PFZ	(Bianchi & Gersonde 2002)
PS2305-6	127.2 ± 1.4	1	127.2	±0.7	1.3*	AZ	(Bianchi & Gersonde 2002)
TPC288	129.3 ± 0.6	1	-	-	-	-	This study
Indian sector							
RC11-120	-	-	128.8	±0.7	13.5*	N of STF	(Martinson et al. 1987)
MD97-2106	-	-	129.8	±0.6	16.1	N of STF	(Cortese et al. 2013)
MD88-770	-	-	123.7	±0.3	11.1	SAZ	(Barrows et al. 2007)
MD02-2488	-	-	129.4	±0.2	13.3*	N of STF	(Govin et al. 2009)
MD97-2108	-	-	127.8	+1.4, -1.5	14.4	N of STF	(Cortese et al. 2013)
MD84-551	-	-	128.9	+1.4,-1.3	6.1*	PFZ	(Pichon et al. 1992)
PS2603-3	124.2 ± 3.2	1	127.4	±0.7	3.8*	PFZ	(Bianchi & Gersonde 2002)
Pacific sector							
DSDP 593	-	-	123.9	+1.6, -3.5	15.1	N of STF	(Cortese et al. 2013)

	Age of MIS 5e Sea Ice Min (ka)	MIS 5e Minimum Sea Ice Conditions	Age of MIS 5e SST peak (ka)	Error on MIS 5e SST peak age (ka)	MIS 5e Peak SST (°C) (*summer SST)	MIS 5e oceanographic zone	References for MIS 5e Conditions
ODP 1123	-	-	118.8	±1.4	17.4	N of STF	(Cortese et al. 2013)
SO136-003	-	-	128.1	+0.5,-0.4	15.4	N of STF	(Barrows et al. 2007)
	-	-	127.6	±0.5	15.6	N of STF	(Cortese et al. 2013)
	-	-	129.8	+0.2,-0.4	19.0	N of STF	(Pelejero et al. 2006)
MD06-2986	-	-	126.1	+1.1, -0.9	16.4	N of STF	(Cortese et al. 2013)
DSDP 594	-	-	123.1	+0.5, -0.9	15.2	N of STF	(Cortese et al. 2013)
	-	-	128.6	±0.5	15.6	N of STF	(Barrows et al. 2007)
MD97-2120	-	-	126.8	±0.8	16.1	N of STF	(Pahnke et al. 2003)
Y9	-	-	121.8	±1.3	12.3	SAZ	(Cortese et al. 2013)
SO136-038	-	-	117.7	±2.8	10.6	SAZ	(Cortese et al. 2013)
MD97-2109	-	-	122.4	+1.4, -1.5	11.6	SAZ	(Cortese et al. 2013)
SO136-111	124.1 ± 6.1	1	127.4	+0.3, -0.8	6.1*	PFZ	(Crosta et al. 2004)
PS58/271-1	127.9 ± 0.4	1	125.8	+0.3, -0.6	3.1*	PFZ	(Esper & Gersonde 2014b, a)

236

Table 2: Published ages and values of MIS 5e peak SSTs with associated errors from the sample resolution (+ indicates younger ages, - indicates older ages). Ages for the MIS 5e minimum in WSIE are given as the centre age of an MIS 5e interval with either FCC <1 % or FCC =0 % (for a core with an MIS 5e interval barren of sea-ice diatoms), with the errors indicating the duration of this interval. The MIS 5e sea ice conditions use the same definitions as Table 1: 1 – core is located north of the maximum winter sea ice limit. The peak MIS 5e SSTs are also given alongside the inferred oceanographic setting, assuming that SSTs at fronts during MIS 5e were similar to those at the modern SO fronts. Cores are listed in the same order as in Table 1. AZ: Antarctic Zone, PFZ: Polar Frontal Zone, SAZ: Subantarctic Zone, STF: Subtropical Front.

237 Frontal Zone, i.e. at 126.8 ± 3.0 ka and 127.3 ± 1.3 ka, respectively (Figure 4). In the Atlantic sector MIS
238 5e SSTs within the ACC and north of the STF reached their peaks all around the same time at 127 ± 1.1
239 ka (Figure 4). The younger average age of MIS 5e peak SSTs in the Subantarctic Zone across the SO is
240 mainly caused by the Pacific sector records (Figure 4). In the Pacific sector cores from the Subantarctic
241 Zone SSTs reached their maximum, at 120.6 ± 2.1 ka, over 5 ka later than in the cores north of the STF
242 and from the Polar Frontal Zone, at 125.9 ± 3.2 ka and 126.6 ± 0.8 ka, respectively.

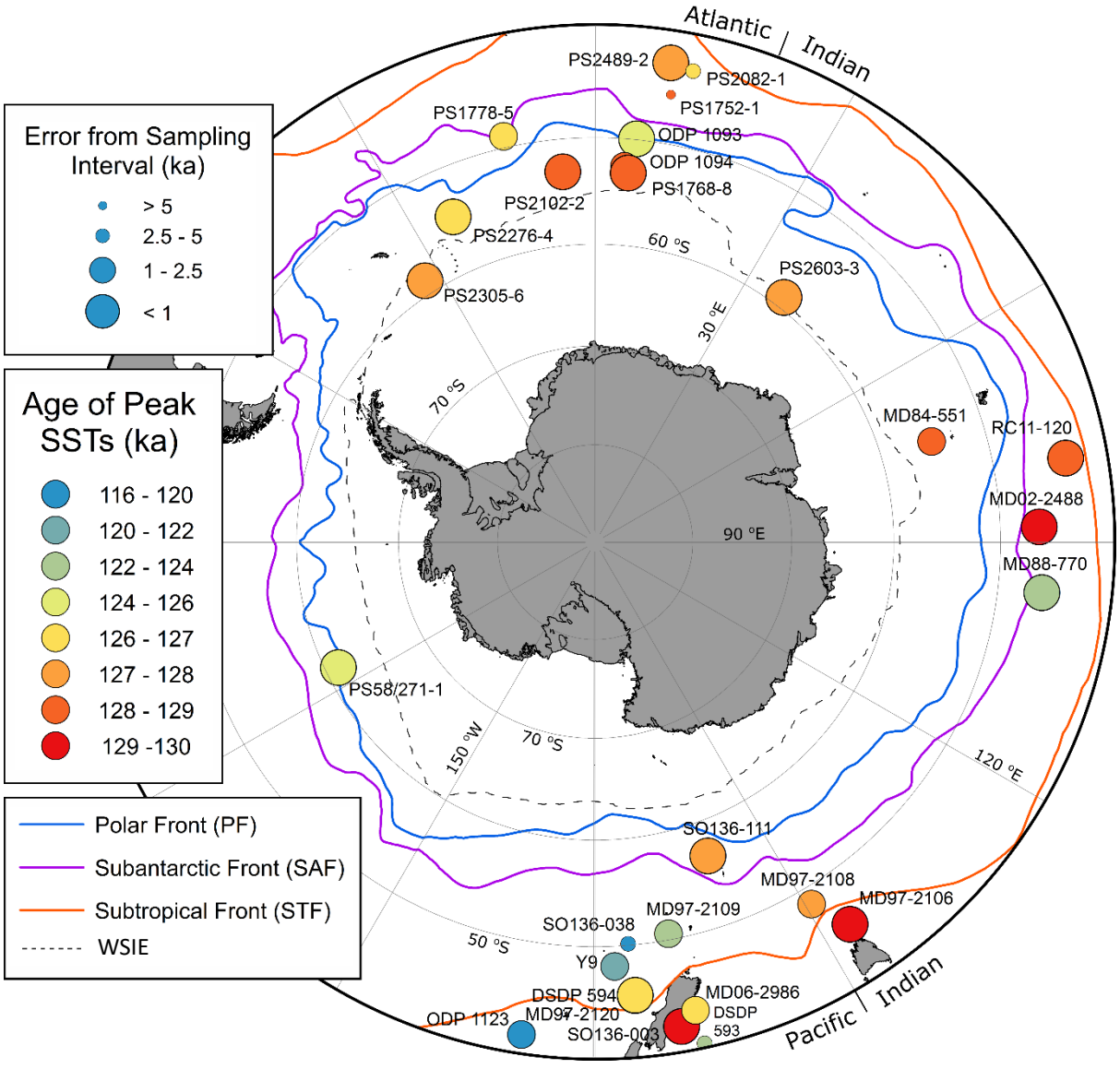

Figure 5: Map of the ages of peak SSTs (colour coded) in the MIS 5e records and the age error (symbol size) arising from the sample resolution for each MIS 5e record. The map covers the region south of 40 °S and includes the modern (1981-2010) average September sea-ice extent and SO frontal positions.

Almost all the core records show increased SSTs during MIS 5e, with the exceptions of cores PS1752-1 and DSDP Site 593, which are characterised by negative SST anomalies of -2 °C and -0.5 °C, respectively. At site PS1752-1 the apparent SST cooling is likely an artefact due to the large age uncertainty caused by the low sample resolution (Tables 1 & 2), whilst the cooling at Site DSDP 593 is probably a consequence of local oceanographic changes during MIS 5e (for details, see Cortese et al. 2013). In the Atlantic sector, only ODP Site 1093 has a peak SST age younger than 129-126 ka (Figure 5). The records from cores MD84-551, MD02-2488 and RC11-120 from the central part of the Indian sector exhibit very similar ages, around 129 ka, for the SST maxima, whilst the peak SST of core MD88-770 lags by ca. 5 ka. Thus, the latter age is clearly an outlier (Figures 3-5) that we excluded from calculating the average time of the MIS 5e SST maximum in the Indian sector. The ages of peak warming in the Pacific sector shows considerable variability, although in the majority of the Pacific sector cores peak MIS 5e SSTs occur after 127 ka (Figures 4 & 5). For the records from the Atlantic and Indian sectors, the average sampling interval error is ~ 0.8 ka, whereas the Pacific sector cores have an average sampling resolution error of ~ 1.1 ka (Figure 5). Core PS1752-1 from the Atlantic sector is the only record, for which the error associated with the sample resolution is greater than the error arising from its age model.

MIS 5e SST maxima and their anomalies relative to the modern SSTs are higher at lower latitudes (Figure 6a). Peak MIS 5e SSTs of > 10 °C and anomalies > 3 °C relative to the present, with the exception of core MD84-551, are only reconstructed from cores located north of 50 °S (Figure 6). Cores located 2° south of the modern STF show the greatest warming during MIS 5e relative to the present (e.g. MD97-2108, DSDP 594, MD97-2120 and PS2082-1). In cores, which are located in the same SO sector and oceanographic zone, but for which MIS 5e SSTs were reconstructed using different techniques, peak SSTs have similar ages (Figure 5) and are comparable (Figure 6b; e.g. RC11-120 and MD02-2488). The variability of peak SSTs regarding their ages (Figures 3-5), deviations from present (Figure 6a) and absolute values (Figure 6b) observed across the SO during MIS 5e is primarily related to the core site location (oceanographic zone, SO sector) but not the SST reconstruction technique. This is indicated

by the variation in peak SST values, anomalies and ages in Pacific sector cores north of 51 ^{o}S (Figures 5 & 6), all of which were reconstructed using the same technique.

6.2. Sea Ice

The records suggest that the age of the MIS 5e WSIE minimum, defined by the centre age of an MIS 5e interval with either FCC <1 % or FCC =0% (for a core with an MIS 5e interval barren of sea-ice diatoms), occurred during the time window 129-125 ka, when mean and even maximum WSIE were restricted to south of each site at least at one point (Figure 7). The onset of the WSIE minimum precedes the SST maximum within each record, except for core PS2603-3, in which both seem to coincide. This sequence is particularly suggested by the data from sites PS2276-4 and PS58/271-1, where the ages of sea ice minima and peak SSTs are precisely constrained, but where, as in the majority of the records, the sea-ice diatom abundance throughout MIS 5e is very low (Figure 7). The FCC record for core TPC288 (Figure 7) has a pronounced minimum at ~ 129 ka. The interval of the WSIE minimum is shorter for TPC288 than for most of the other records. The minimum FCC in the MIS 5e sediments of core TPC288 does not fall to 0% but is still below the 1% threshold that marks the northern edge of maximum WSIE. Both cores TPC288 and PS2305-6 show a large increase in FCC abundance, from <1 % to ~8 % later during MIS 5e. The FCC maximum in both cores occurs ca. 4-5 ka after the end of the WSIE minimum (Figure 7).

6.3. Oceanographic Fronts

Almost all the records show increased SSTs during MIS 5e, which suggests that the oceanographic fronts were positioned further poleward than at present (Brathauer & Abelmann 1999, Benz et al. 2016). The MIS 5e frontal positions (Table 3 & Figure 6b) are inferred from the reconstructed SSTs (cf. Bianchi & Gersonde 2002), assuming the same temperature relations across the fronts as in the modern ocean (Orsi et al. 1995, Sikes et al. 2002, Meinen et al. 2003, Dong et al. 2006). The frontal positions inferred for MIS 5e are shown alongside the reconstructed MIS 5e SST maxima and

anomalies in Figure 6. These reconstructed frontal positions are solely based on the reconstructed peak SSTs for the cores presented here, and thus only cover small spatial areas (Table 3). In the Pacific sector, where almost all available records are located near New Zealand (between 160 °E and 170 °W), only MIS 5e SST data from a single core (PS58/271-1) are available from the eastern Pacific sector of the SO (170 °W - 65 °W). It is important to acknowledge that, if the entire SO was evenly warmed during MIS 5e relative to the present, then it could give the impression of frontal movement without requiring any actual latitudinal shift of the boundaries between surface water masses. This limitation in the use of SSTs (or sea-surface height) to determine frontal shifts has been taken into account by Gille (2014).

If the reconstructed SSTs are an accurate indicator of frontal location, then the SO fronts were positioned between 1° and 5° further south during MIS 5e when compared to their modern locations, which is consistent with previous reconstructions (Bianchi & Gersonde 2002) (Table 3). The fronts are best constrained for the SE Atlantic sector (30 °W – 15 °E), where the MIS 5e latitudinal ranges of all three fronts show no overlap with those defined by modern SSTs or sea-surface height (Dong et al. 2006, Sokolov & Rintoul 2009) (Table 3).

	Modern, hydrographic sections (Orsi et al. 1995)	**Modern, sea-surface height (Sokolov & Rintoul 2009)**	**MIS 5e (this study)**
30 °W – 15 °E STF	38 – 43 °S	-	43 – 45 °S
30 °W – 15 °E SAF	45 – 48 °S	41 – 48 °S	49 – 51 °S
30 °W – 15 °E PF	49 – 53 °S	48 – 55 °S	55 – 57 °S
70 – 100 °E STF	40 – 42 °S	-	45 – 48 °S
70 – 100 °E SAF	45 – 49 °S	43 – 51 °S	49 – 52 °S
70 – 100 °E PF	48 – 53 °S	56 – 59 °S	S of 56 °S
140 – 180 °E STF	45 – 48 °S	-	46 – 51 °S
140 – 180 °E SAF	52 – 58 °S	50 – 60 °S	52 – 58 °S
140 – 180 °E PF	55 – 62 °S	55 – 64 °S	S of 57 °S

Table 3: Inferred MIS 5e frontal positions in the three SO sectors and modern latitudinal ranges of the frontal positions. The modern positions are given as defined by hydrographic sections (Orsi et al. 1995) and sea-surface height (Sokolov & Rintoul 2009). The former definition utilises hydrographic data up to 1990 and the SSH definition utilises weekly data from 1992-2007.

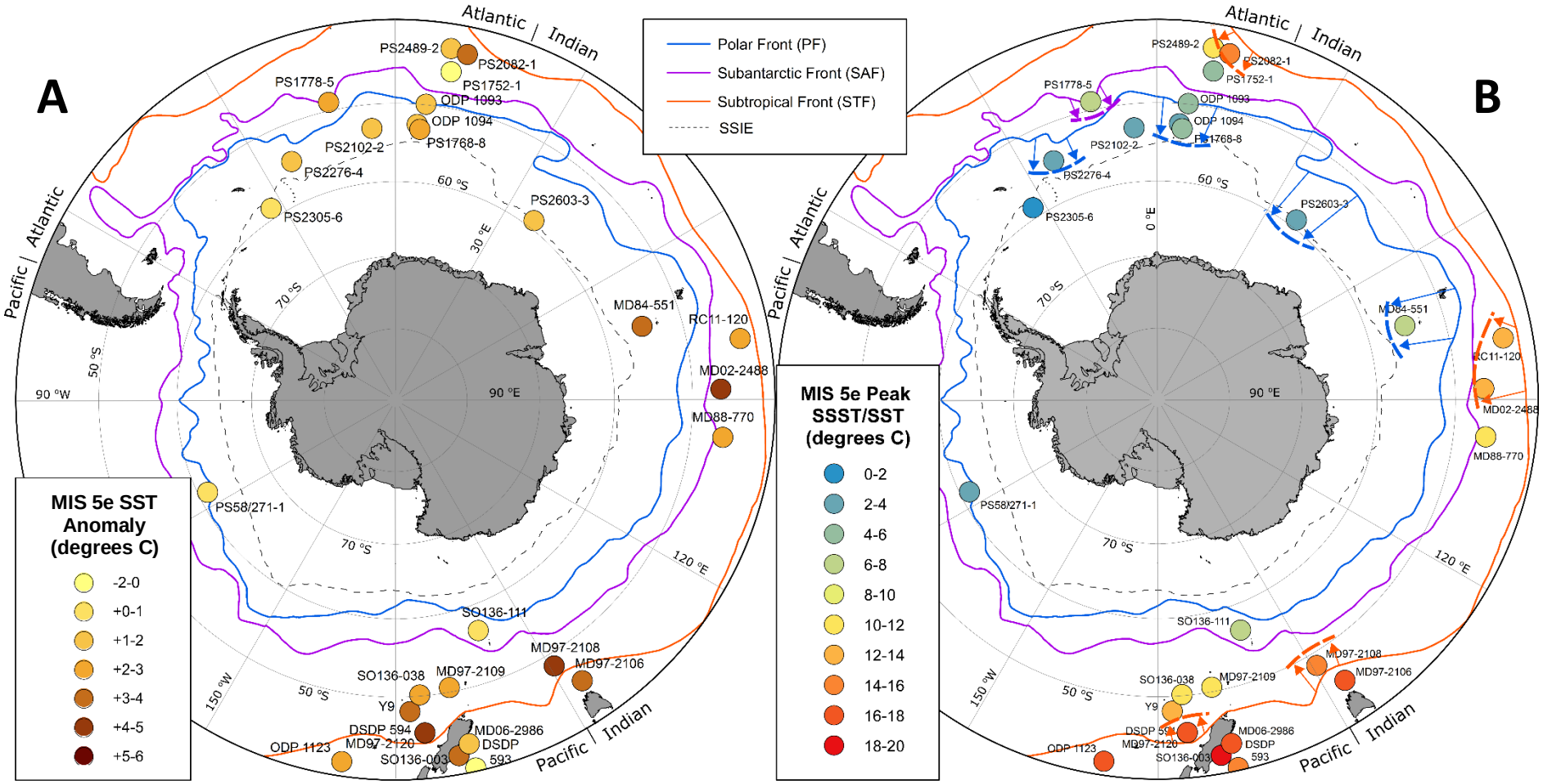

Figure 6: A - Map with SST anomalies relative to the present for the MIS 5e records. **B** - Map with SST maxima for the MIS 5e records and inferred MIS 5e frontal positions (dashed lines) and their shifts relative to the modern positions (arrows). Both maps show the region south of 40 °S, modern SO frontal positions (continuous lines) and average September sea-ice extent for 1981-2010 (grey dashed lines). The PF shift south of core MD84-551 may be an artefact of SST over-estimation at this site (Pichon et al. 1992).

310

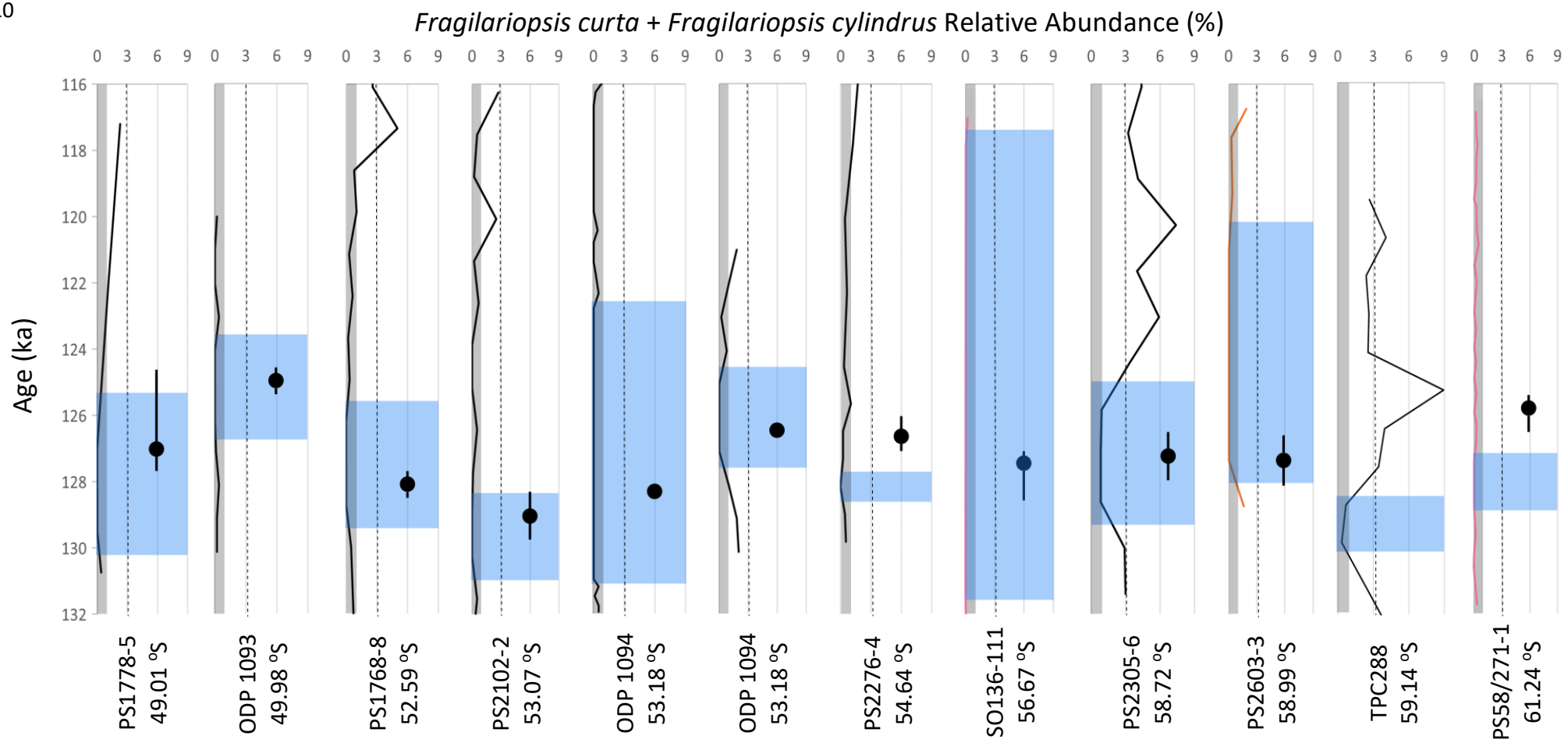

Figure 7: *Fragilariopsis curta* and *F. cylindrus* (FCC) downcore abundances for 11 previously published MIS 5e records from the SO and the new record from core TPC288. Black lines mark the Atlantic sector records, pink lines (SO136-111 and PS58/271-1) the Pacific sector records and the orange line the only Indian sector record (PS2603-3). Blue shading marks the period of minimum WSIE, where the lowest FCC abundances are recorded. The dotted line indicates the 3% threshold for mean WSIE and the grey shading marks the 1% threshold for maximum WSIE (Gersonde & Zielinski 2000, Gersonde et al. 2003, Gersonde et al. 2005). The black dots mark ages of peak SSTs in each published record with error bars arising from the sample resolution. Records are ordered from north to south.

7. Discussion

7.1. Sea Surface Temperatures

The peak SO warming during MIS 5e seems to occur asynchronously in the three sectors. In the Atlantic and Indian sectors, the SST maxima have well constrained ages of 127.4 ± 1.1 ka and 128.7 ± 0.8 ka, respectively, which are, however, within age-model error of each other and therefore we cannot exclude the possibility that both SST maxima occurred concurrently. The SST record for core MD88-770 (Barrows et al. 2007) is an average of three different transfer function methodologies, with reconstructed SSTs varying between the methods by 0.3-2 ^{o}C during MIS 5e, and shows an anomalously late SST peak relative to the other cores from the central part of the Indian sector (RC11-120, MD84-551 and MD02-2488). However, it is worth noting that the artificial neural network derived SST record of Barrows et al. (2007) has an older maximum, with an age similar to that of the SST peaks in the other three cores. The ages of peak SSTs in the Pacific sector vary considerably, from 129.8 ka to 117.7 ka and in most cores from this sector, particularly those from the MIS 5e Subantarctic Zone (Figure 5), they seem to lag those of the peak SSTs in the Atlantic and Indian sectors. Average ages of MIS 5e peak SSTs for the different sectors lie within 3 ka (128-125 ka, see Figure 3), which is within the uncertainty of the LR04 chronology. Therefore, within error, the MIS 5e SST maxima appear to occur synchronously in all sectors. However, whilst the offset in timing of peak SSTs between the Atlantic and Indian sectors is ~ 1.5 ka, SST maxima in several Pacific sector cores occurred over 3 ka later than in the Atlantic and Indian sector cores.

The three Pacific sector records from the MIS 5e Subantarctic Zone (MD97-2120, Y9 and SO136-038) are all located on the Campbell and Bounty Plateaus, south of New Zealand. These plateaus are overlain by highly stratified and thermally isolated surface waters (Neil et al. 2004). This isolation, coupled with the northward influx of colder waters along the Pukaki Saddle (Neil et al. 2004, Cortese et al. 2013) could explain the later age of peak SSTs observed in the three records.

335 Antarctic air temperature, documented in isotope records from East Antarctic ice cores (Masson-
336 Delmotte et al. 2011, Holloway et al. 2017), reaches a maximum at 127.7 ka. The ice-core chronologies
337 have an uncertainty of 1.5 ka during MIS 5e (Bazin et al. 2013) and therefore only the Pacific sector
338 reaches maximum SSTs later than peak Antarctic air temperatures during MIS 5e (Figure 8). For the
339 Atlantic and Indian sectors the ages of peak atmospheric and oceanic temperatures overlap within
340 error.

341 To explore the forcing of maximum SSTs during MIS 5e we compare the timing of insolation changes
342 with the peak SST ages. The ages of maximum SSTs in the three SO sectors do not match that of peak
343 austral summer insolation (monthly mean for January at 55 ^{o}S), which reaches a minimum between
344 130 and 120 ka (Figure 8). The SST maximum in the Atlantic sector coincides closely with peak austral
345 winter insolation (July monthly mean) at 55 ^{o}S and occurs earlier than peak boreal summer insolation
346 (July monthly mean) at 55 ^{o}N (Figure 8). Boreal summer insolation is predicted to drive SO warming
347 via the 'bipolar seesaw' mechanism, whereby increased boreal insolation causes substantial melting
348 and freshwater release from the northern hemisphere ice sheets (Marino et al. 2015). This large
349 freshwater release results in reduced North Atlantic overturning and an associated warming of the SO
350 (Stocker & Johnsen 2003, Marino et al. 2015). The MIS 5e SST maxima in the Pacific and Indian sectors
351 do not seem to match any of the southern hemisphere insolation peaks (Figure 8). The peak SST age
352 in the Pacific sector matches that of the insolation peak for boreal summer (July at 55 ^{o}N) but the
353 mechanism behind this concurrence is unknown.

354 Currently, there are not enough marine MIS 5e records from the SO to test the statistical significance
355 of the temporal offsets between peak SSTs in the three SO sectors, but the ages of the SST maxima
356 appear to have occurred earliest in the Indian and Atlantic sectors followed by the Pacific sector. It is
357 unclear whether this sequence is consistent with the 'bipolar seesaw' model of SO warming during
358 MIS 5e proposed by Holloway et al. (2017) due to the uncertainties in the age models. However it does

359

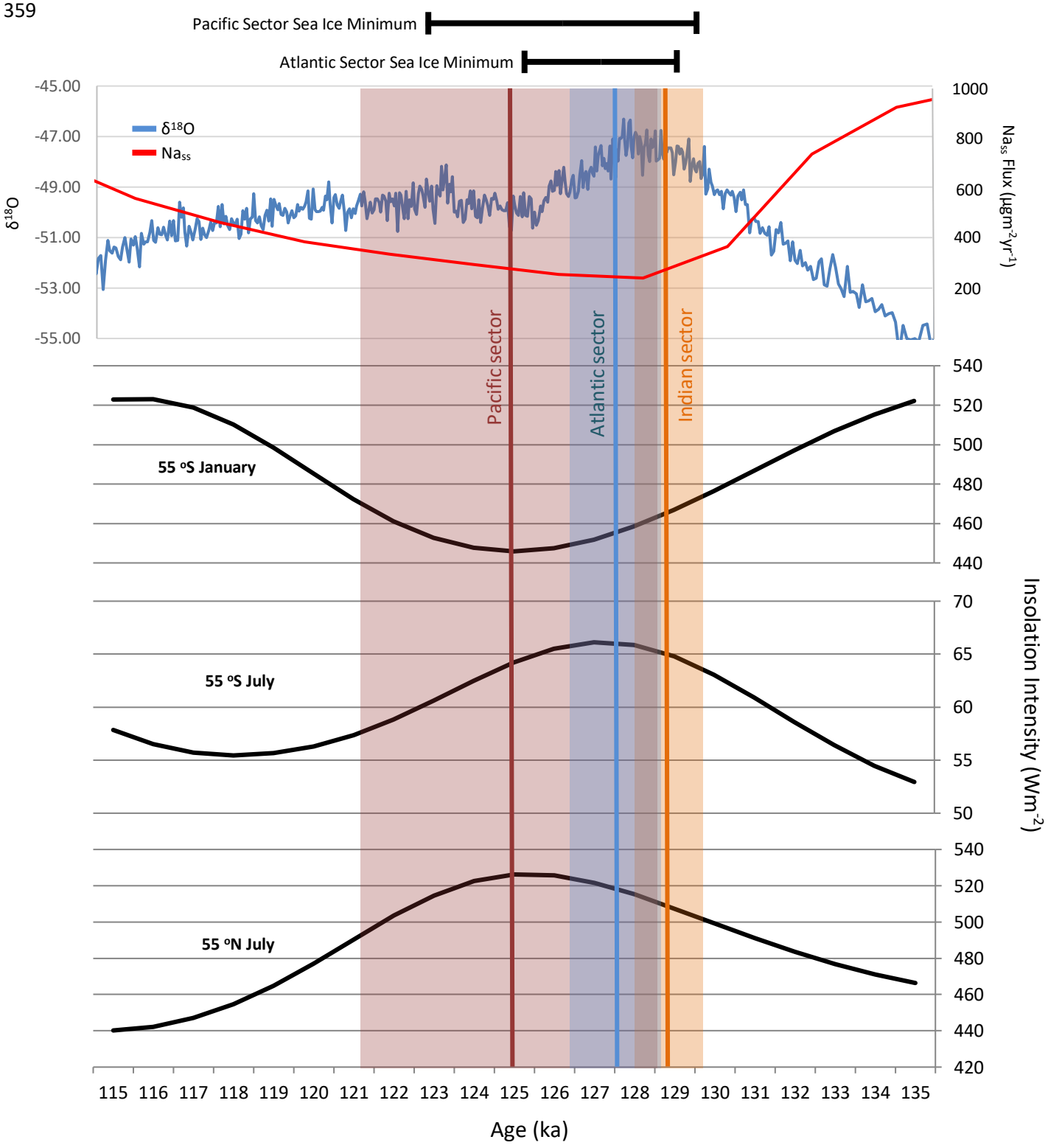

Figure 8: EPICA Dome C $\delta^{18}O_{ice}$ (Masson-Delmotte et al. 2011) and Na_{ss} flux (Wolff et al. 2006) records and insolation intensity for the time period 135 – 115 ka (all converted onto the LR04 chronology). The insolation intensities are January or July means for latitudes at 55 °S and 55 °N. The average age of the MIS 5e SST maximum for each SO sector is marked by a vertical line (Red – Pacific sector, Blue – Atlantic sector, Orange – Indian sector), with the standard deviation marked by the shaded area of corresponding colour. The average and standard deviation for the Indian sector was calculated excluding the SSTs from site MD88-770. The average age ranges of the MIS 5e sea-ice minima in the Atlantic and Pacific sectors are also marked.

seem to suggest the intriguing possibility of other unknown mechanisms, if indeed the SSTs in the Pacific sector reached their maximum later than in the Indian and Atlantic sectors.

7.2. Sea Ice

Although many of the core records are located too far north to give a precise age for the MIS 5e WSIE minimum, its reconstructed temporal range is largely consistent with an average age of 129-125 ka at the beginning of MIS 5e. Notably, with the exception of ODP Site 1093, the WSIE minima of all records (Figure 7) coincide with the minimum in sea salt sodium (Na_{ss}) flux in the East Antarctic EPICA Dome C ice core at ~128 ka (Wolff et al. 2006). Comparisons between the ages of peak SSTs and WSIE minima show that for most cores the peak SSTs occurred within the interval of minimum WSIE. Within a SO sector, the time of peak SST may actually coincide with the time of the absolute WSIE minimum, as is suggested by the poleward progression of the WSIE minimum in the Atlantic sector during deglacial warming across Termination I (Xiao et al. 2016). Exceptions may be cores PS2276-4 and PS58/271-1, where the minimum WSIE intervals are better constrained and seem to suggest that minimum WSIE preceded peak SSTs during MIS 5e (Figure 7). However, the abundances of sea-ice diatoms in both of these cores are <1 % throughout most of MIS 5e (Figure 7), and therefore more southerly cores with precise ages for the minimum WSIE during MIS 5e are required to further analyse any possible lead/lag between peak SSTs and minimum WSIE.

The new sea ice record from core TPC288 has a more precisely constrained minimum than most of the previously published records and shows an early WSIE minimum (Figure 7). The FCC abundance values >0 % in cores PS2305-6 and TPC288 suggest that the sea-ice cover during the MIS 5e minimum reached further north in the Scotia Sea than in the Amundsen Sea (PS58/271-1). The WSIE in the Scotia Sea also shows an earlier resurgence following the minimum, with FCC abundances in cores TPC288 and PS2305-6 rising to ~ 8% within only 4-5 ka (Figure 7). Both these cores show similar trends in FCC abundances after the minimum, with a temporal offset likely due to age model uncertainties or unconstrained changes in sedimentation rate between tie-points.

385 If the sea ice minimum exactly coincided with the Na_{ss} flux minimum at 128 ka, then it would have
386 preceded the peak SSTs in the Atlantic sector, although this offset is within age model errors. Currently
387 there are only three sea ice records available from outside the Atlantic sector, so it is difficult to draw
388 robust conclusions on the relative timing of the WSIE minima between the three sectors. The records
389 from the Pacific sector (SO136-111 and PS58/271-1) and the Indian sector (PS2603-3) exhibit WSIE
390 minima during similar time intervals as the Atlantic sector records (Figures 6 and 8), so it appears the
391 MIS 5e WSIE minimum occurred largely synchronously throughout the SO.

392 The age ranges for the WSIE minima during MIS 5e encompass the 127 ka-insolation peak for austral
393 winter (July mean) at 55 ^{o}S (Figure 8). Peak austral winter insolation results in a milder and shorter
394 austral winter with less sea ice formation, whilst the nearly coinciding minimum in austral summer
395 insolation (January mean at 55 ^{o}S) is characterised by a cooler but longer austral summer, resulting in
396 increased sea-ice melt back, as is supported by model results of Huybers & Denton (2008). The peak
397 in austral winter insolation could therefore have driven Antarctic sea ice retreat at 127 ka.

398 The possible importance of shorter austral winter duration with milder July temperatures in the timing
399 of the WSIE minimum during MIS 5e might explain the seeming decoupling between the timing of the
400 WSIE minimum and peak SSTs in cores PS2276-4 and PS58/271-1 (Figure 7). For both of these cores
401 the SST records are summer SSTs, not annual SSTs, and thus do not incorporate the potentially crucial
402 winter SSTs. The peak in summer SSTs may reflect a period of increased seasonality, with warmer
403 summers and cooler winters, rather than the period when annual SSTs were highest for MIS 5e. There
404 is also the possibility that the transfer functions used to reconstruct summer SSTs during MIS 5e are
405 sensitive to events of a different frequency or magnitude than those recorded in the FCC abundances.

406 ### 7.3. Oceanographic Fronts

407 The reconstructed peak SSTs during MIS 5e were higher than today, suggesting more southerly frontal
408 positions in the SO. The inferred latitudinal shifts of the MIS 5e frontal positions, when compared with

409 the present, assume that the SST characteristics of SO surface water masses are the same as the
410 modern during MIS 5e. These latitudinal shifts vary substantially, with some fronts (e.g. STF at 30 °W
411 – 15 °E) having shifted by only 1° and others (e.g. PF at 30 °W – 15 °E) having shifted by 5°. The
412 differences in the latitudinal frontal shifts could be related to bathymetric constraints. For example,
413 Moore et al. (1999) showed that the latitudinal position of the present day PF in areas without such
414 constraints varies considerably on seasonal and annual timescales but that such variations are reduced
415 in areas where bathymetric features "pin" the frontal position. Notable areas, where fronts are
416 pinned, include Drake Passage, Kerguelen Plateau and the Pacific-Antarctic Ridge (e.g. Orsi et al. 1995).
417 Thus, core sites located close to these regions probably recorded only very limited shifts of frontal
418 positions during MIS 5e.

419 The overall concentric geographical pattern of the SO fronts was the same during MIS 5e as today,
420 with the reconstructed frontal positions between 140 °E and 180 °E located more southerly than in
421 other regions, and the fronts between 30 °W and 15 °E located at the most northerly positions when
422 compared to other regions (Table 3). However, the MIS 5e frontal positions are averages for each
423 region (Table 3) and only represent a limited geographical coverage of the entire SO. Therefore, they
424 may not be an accurate representation of the full latitudinal range of frontal position shifts during the
425 MIS 5e climatic optimum. This is particularly true for the Pacific sector, where there is considerable
426 spatial bias in the distribution of available records, with only a single MIS 5e SST record being available
427 from the area between 65 °W and 170 °W. The reconstructions of frontal positions are also potentially
428 biased by the proxy records, which can exacerbate the actual SST signal. This is evident from the +2.5°C
429 over-estimation of the modern SST by the diatom assemblage inferred SST from core-top sediments
430 at site MD84-551 (Pichon et al. 1992). SST over-estimation due to proxy is also indicated for the MIS
431 5e SST maximum at site SO136-003, for which Pelejero et al. (2006) reconstructed 19.6 °C, whereas
432 Barrows et al. (2007) and Cortese et al. (2013) concluded SST maxima of only 16.24 °C and 16.4 °C,
433 respectively. The higher SST reconstructed by Pelejero et al. (2006) used the biomarker proxy $U^{K'}_{37}$,
434 which - similar to Mg/Ca ratios measured on calcareous shells of planktonic foraminifera - produces

435 warmer SSTs than microfossil assemblages (Hoffman et al. 2017) and which reproduces less accurate
436 modern SSTs in regions with cool surface waters (Filippova et al. 2016). However, most of the SST
437 proxy records reported here use microfossil transfer functions, and so the risk of any bias in the SST
438 values is minimal, which suggests the frontal positions reconstructed for MIS 5e are reliable, even if
439 the absolute SST values are not. The type of microfossil group used in the MIS 5e SST reconstructions
440 has no impact on the timing of the peak SSTs.

441 The differences between the MIS 5e and the modern SSTs are largest (>3 °C) in the region between 45
442 °S and 49 °S and between 140 °E and 180 °E (Figure 6a). This is interpreted as a consequence of the
443 STF location in this region having shifted south of 46 °S during MIS 5e, i.e. at least 1° further south
444 than at present (Figure 6b). The MIS 5e shifts in the STF position are associated with the largest SST
445 anomalies due to the greater thermal gradient across this front when compared to the SAF and PF
446 (Orsi et al. 1995). In the Atlantic sector the ages of peak MIS 5e SSTs within the four oceanographic SO
447 zones are all coeval within the age model errors (Figure 4). This suggests that the SST maxima and
448 most poleward ACC frontal positions during MIS 5e were reached at the same time within this sector.
449 SSTs north of the STF and in the Polar Frontal Zone of the Indian and Pacific sectors peaked around
450 the same time (Figure 4). SSTs in the Subantarctic Zone of the Pacific sector reached their maxima 3-
451 7 ka later than in the other sectors and other oceanographic zones (Figure 4).

452 Although the peak SST during MIS 5e was higher than the present day SST at almost every core site,
453 the positive SST anomalies vary between 0.1 °C and 5.2 °C (Figure 6a). The lack of consistent SST
454 increases may result from some cores having been affected by the same surface water mass during
455 both the present and MIS 5e (e.g. PS2305-6, SO136-003 and PS58/271-1), whereas others were bathed
456 by different surface water masses during these times (e.g. DSDP Site 594, MD97-2108 and MD84-551).
457 Variability of SST anomalies between core sites across the SO and within the same SO sector
458 strengthen the argument that the higher SSTs during MIS 5e are associated with the poleward shift of
459 the SO fronts and associated water masses. If the entire SO warmed evenly and independently of any

change in the location of a front (Gille 2014) then the SST anomalies should be more consistent between sites, at least between sites from the same SO sector. High latitude sites south of 55 °S have MIS 5e SST anomalies <1 °C, which may suggest that MIS 5e warming closer to the Antarctic continent was less pronounced than north of the PF. However, the observed slight trend towards higher SST anomalies at more northerly SO sites than at sites nearer to the Antarctic continent may be an artefact caused by the higher SST anomalies being associated with the southward shift of the STF (Figure 6b).

7.4. Wider Implications

The high SST maxima and inferred poleward shifts of the SO fronts during MIS 5e must have had impacts on both the Antarctic region and further afield. The more southerly position of the ACC fronts was compatible with a poleward shift in the westerly wind field, which would have resulted in a more southerly precipitation field and storm tracks (Russell et al. 2006, Liu & Curry 2010). More southerly storm tracks would have increased sea ice break up and promoted a reduced annual sea ice duration and extent (Hall & Visbeck 2002). The precipitation field shift would also have resulted in reduced precipitation in regions like southern Australia and increased precipitation closer to Antarctica (Fletcher & Moreno 2011, Saunders et al. 2012). Changes in the precipitation sources and fields also have an effect on the interpretation of ice core records because they can affect the air temperature signature of water isotopes (Masson-Delmotte et al. 2011).

A more southerly and warmer ACC would also cause increased warming of the continental shelves around Antarctica with anomalous bottom Ekman flow (Spence et al. 2017), causing increased advection of relatively warm ACC water masses, such as Circumpolar Deep Water, onto the Antarctic continental shelf (Fogwill et al. 2014). Increased warm water upwelling would have increased melting of floating ice shelves (Ronne-Filchner, Ross, Amery etc.) and at grounding zones of marine-terminating ice streams around Antarctica which, in turn, would have caused major mass loss from the Antarctic ice sheets (Pollard & DeConto 2009, DeConto & Pollard 2016), similar to what has been observed along the Pacific margin of Antarctica today (Jenkins et al. 2016, Shepherd et al. 2018, Rignot

et al. 2019) and since the last ice age (Hillenbrand et al. 2017). Intrusions of warm water into the Weddell Sea might have caused significant reduction in sea ice formation, given the high rates of sea ice production in this area today (Haid & Timmermann 2013), as well as considerable loss of glacial ice (Hellmer et al. 2012). Warming of Weddell Sea waters and the poleward shift of the northern boundary of the Weddell Gyre (Orsi et al. 1995) would also have reduced the extent of the Weddell Gyre circulation whilst increasing its strength (Wang 2013). A similar scenario can also be assumed for the Ross Sea Gyre.

A poleward shift of the STF would have increased the flow in counter currents, such as the Agulhas Current, that would therefore increase the influx of warmer Indian Ocean waters into the South Atlantic (Biastoch et al. 2009). Other boundary currents, such as the East Australian Current, would also have been able to expand, and this current may have changed its flowpath from north of Chatham Rise to the south of it (Cortese et al. 2013). In contrast, the Brazil Current is unlikely to have changed substantially and shifted its flowpath into Drake Passage because of the inability of the ACC to be displaced substantially poleward through that region (Mazloff 2012). Changes in the boundary currents and fronts would have impacted not only the oceanic conditions but also have influenced ecosystems within the SO and adjacent ocean basins. An example of this is the effect of an increased Agulhas Current flow that would have injected more warmth into the South Atlantic and reduced nutrient availability, substantially damaging biological productivity in the cold water Benguela Current (Hutchings et al. 2009, Tim et al. 2018).

The reduced sea-ice extent in the SO during MIS 5e would have influenced deep and bottom water formation around Antarctica. A reduction in the extent of sea ice (and possibly also of ice shelves, see above) would have resulted in less formation of dense shelf waters by brine rejection (and by super-cooling in ice-shelf cavities), which in turn would have reduced the rate of deep and bottom water mass production in the SO and caused a subsequent warming of abyssal waters (Armand & Leventer 2003, Ferrari et al. 2014). Reductions in formation of southern-sourced cold deep and bottom waters

would have had far reaching consequences for the water column structure of the World Ocean. This is because the reduction of SO deep- and bottom water masses probably resulted in a slowdown of SO circulation and therefore Atlantic Meridional Overturning Circulation, which in turn may have delayed the re-initiation of North Atlantic Deep Water formation, following its initial shutdown at the beginning of MIS 5e due to meltwater stratification in the North Atlantic (Marino et al. 2015, Holloway et al. 2017). The possible impact of sea-ice decrease in the SO on North Atlantic Deep Water formation gives evidence of its importance for global ocean and atmosphere interactions, and how crucial it is to gain a better understanding of past changes for predicting future changes.

8. Conclusions

The available SST records from the SO indicate that the SST maximum during MIS 5e in the Atlantic, Indian and Pacific sectors occurred on average at 127.4 ± 1.1 ka, 128.7 ± 0.8 ka and 124.9 ± 3.6 ka, respectively. Whilst SSTs seem to have peaked simultaneously within the age uncertainties in all three sectors, the maximum SSTs in several records from the Pacific sector occurred much later than in those from the Atlantic and Indian sectors, suggesting that peak warming was not synchronous throughout the SO. The low number and limited geographical coverage of records prevents statistical analyses. Nonetheless, the peak SST ages from cores in the Atlantic and Indian sectors indicate that maximum SSTs there were reached concurrently with peak atmospheric temperatures measured in Antarctic ice cores (127.7 ka).

The age ranges for MIS 5e sea ice minima in the SO are consistent with ice core proxy-based estimates of sea-ice extent but there is a clear need for more marine records from the Antarctic Zone to better constrain the exact timing and position of minimum sea-ice extent during MIS 5e. Better constrained ages for minimum WSIE will help to interrogate whether an observed temporal offset between peak SSTs and minimum WSIE in cores PS2276-4 and PS58/271-1 is an artefact or not. The addition of the new sea ice record from site TPC288 constrains the WSIE minimum at this site to 129.3 ± 0.6 ka, consistent with the previously published records from the Atlantic sector. Despite the paucity of

records from the Indian and Pacific sectors, the WSIE minimum appears to have been synchronous throughout the SO.

The Subtropical, Subantarctic and Polar Fronts were potentially situated at least 1^{o} further south than today during MIS 5e, and accompanying poleward shifts of surface water masses are inferred from SSTs that were considerably higher during MIS 5e than at present. However, the large latitudinal variations in frontal positions observed today, both within a particular SO sector and on a seasonal and annual time scales, make it difficult to accurately reconstruct the ACC structure during MIS 5e based on a limited and geographically restricted number of records. The relatively high number of records from the Atlantic sector, the coherency of the latitudinal temperature gradient reconstructed for these records, and the absence of bathymetric constraints in this region indicate that the MIS 5e frontal migrations there are the most robust.

The proxy records compiled here provide data that can constrain model experiments and test their results. Evaluating numerical models, which simulate the processes operating under a warmer climate, such as during MIS 5e, with palaeo-data as compiled in this study, will help improve confidence in predictions of future climate change. The MIS 5e records reveal potential heterogeneity in SO warming and sea ice reduction that can be used to evaluate the significance of processes built into models, such as deep- and bottom-water formation and overturning circulation.

Data Availability

Datasets related to this article can be found at http://dx.doi.org/10.17632/sb5ybjhxs5.1 and http://dx.doi.org/10.17632/9x86z33vzm.1, open-source online data repositories hosted at Mendeley Data (Chadwick 2019a, b).

Declaration of interest

Conflict of interest: none

Acknowledgements

We thank Sarah Humbert and James Kershaw for technical assistance with the Analyseries software. This work forms part of the BAS Polar Science for Planet Earth program. We furthermore thank Xavier Crosta and an anonymous referee for their constructive reviews, which helped improve this paper.

Funding

This work was supported by the Natural Environmental Research Council [grant number NE/L002531/1].

References

Allen C.S. 2014. Proxy development: a new facet of morphological diversity in the marine diatom Eucampia antarctica (Castracane) Mangin. Journal of Micropalaeontology, **33**(2): 131-142.

Armand L. & Leventer A. (2003). Palaeo Sea Ice Distribution - Reconstruction and Palaeoclimatic Significance. Sea Ice: An Introduction to its Physics, Chemistry, Biology and Geology**:** 333-372.

Bakker P., Masson-Delmotte V., Martrat B., Charbit S., Renssen H., Gröger M., Krebs-Kanzow U., Lohmann G., Lunt D.J., Pfeiffer M., Phipps S.J., Prange M., Ritz S.P., Schulz M., Stenni B., Stone E.J. & Varma V. 2014. Temperature trends during the Present and Last Interglacial periods – a multi-model-data comparison. Quaternary Science Reviews, **99**: 224-243.

Barrows T.T., Juggins S., De Deckker P., Calvo E. & Pelejero C. 2007. Long-term sea surface temperature and climate change in the Australian-New Zealand region. Paleoceanography, **22**(2): PA2215.

Bazin L., Landais A., Lemieux-Dudon B., Toyé Mahamadou Kele H., Veres D., Parrenin F., Martinerie P., Ritz C., Capron E., Lipenkov V., Loutre M.F., Raynaud D., Vinther B., Svensson A., Rasmussen S.O., Severi M., Blunier T., Leuenberger M., Fischer H., Masson-Delmotte V., Chappellaz J. & Wolff E. 2013. An optimized multi-proxy, multi-site Antarctic ice and gas orbital chronology (AICC2012): 120–800 ka. Climate of the Past, **9**(4): 1715-1731.

Becquey S. & Gersonde R. 2003. A 0.55-Ma paleotemperature record from the Subantarctic zone: Implications for Antarctic Circumpolar Current development. Paleoceanography, **18**(1): 1014-1028.

Belkin I.M. & Gordon A.L. 1996. Southern Ocean fronts from the Greenwich meridian to Tasmania. Journal of Geophysical Research: Oceans, **101**(C2): 3675-3696.

Benz V., Esper O., Gersonde R., Lamy F. & Tiedemann R. 2016. Last Glacial Maximum sea surface temperature and sea-ice extent in the Pacific sector of the Southern Ocean. Quaternary Science Reviews, **146**: 216-237.

Bianchi C. & Gersonde R. 2002. The Southern Ocean surface between Marine Isotope Stages 6 and 5d: Shape and timing of climate changes. Palaeogeography, Palaeoclimatology, Palaeoecology, **187**: 151-177.

Biastoch A., Boning C.W., Schwarzkopf F.U. & Lutjeharms J.R. 2009. Increase in Agulhas leakage due to poleward shift of Southern Hemisphere westerlies. Nature, **462**(7272): 495-498.

Brathauer U. 1996. Radiolarians as indicators for Quaternary climatic changes in the Southern Ocean (Atlantic Sector). Reports on Polar Research, **216**: 1-163.

Brathauer U. & Abelmann A. 1999. Late Quaternary variations in sea surface temperatures and their relationship to orbital forcing recorded in the Southern Ocean (Atlantic sector). Paleoceanography, **14**(2): 135-148.

Brathauer U., Abelmann A., Gersonde R., Niebler H.-S. & Futterer D.K. 2001. Calibration of *Cycladophora davisiana* events versus oxygen isotope stratigraphy in the subantarctic Atlantic Ocean - a stratigraphic tool for carbonate-poor Quaternary sediments. Marine Geology, **175**: 167-181.

Capron E., Govin A., Feng R., Otto-Bliesner B.L. & Wolff E.W. 2017. Critical evaluation of climate syntheses to benchmark CMIP6/PMIP4 127 ka Last Interglacial simulations in the high-latitude regions. Quaternary Science Reviews, **168**: 137-150.

Capron E., Govin A., Stone E.J., Masson-Delmotte V., Mulitza S., Otto-Bliesner B., Rasmussen T.L., Sime L.C., Waelbroeck C. & Wolff E.W. 2014. Temporal and spatial structure of multi-millennial temperature changes at high latitudes during the Last Interglacial. Quaternary Science Reviews, **103**: 116-133.

Chadwick M. (2019a). Age-model tiepoints for cores DSDP 594, MD88-770, MD02-2488, MD84-551, ODP site 1094, SO136-003, PS1768-8, PS2102-2 and MD97-2120. Mendeley Data.

Chadwick M. (2019b). TPC288 Diatom Abundance for MIS 5e. Mendeley Data.

Cortese G., Dunbar G.B., Carter L., Scott G., Bostock H., Bowen M., Crundwell M., Hayward B.W., Howard W., Martínez J.I., Moy A., Neil H., Sabaa A. & Sturm A. 2013. Southwest Pacific Ocean response to a warmer world: Insights from Marine Isotope Stage 5e. Paleoceanography, **28**(3): 585-598.

Crosta X., Sturm A., Armand L. & Pichon J.-J. 2004. Late Quaternary sea ice history in the Indian sector of the Southern Ocean as recorded by diatom assemblages. Marine Micropaleontology, **50**(3-4): 209-223.

DeConto R.M. & Pollard D. 2016. Contribution of Antarctica to past and future sea-level rise. Nature, **531**(7596): 591-597.

Dong S., Sprintall J. & Gille S.T. 2006. Location of the Antarctic Polar Front from AMSR-E Satellite Sea Surface Temperature Measurements. Journal of Physical Oceanography, **36**: 2075-2089.

Esper O. & Gersonde R. 2014a. New tools for the reconstruction of Pleistocene Antarctic sea ice. Palaeogeography, Palaeoclimatology, Palaeoecology, **399**: 260-283.

Esper O. & Gersonde R. 2014b. Quaternary surface water temperature estimations: New diatom transfer functions for the Southern Ocean. Palaeogeography, Palaeoclimatology, Palaeoecology, **414**: 1-19.

Ferrari R., Jansen M.F., Adkins J.F., Burke A., Stewart A.L. & Thompson A.F. 2014. Antarctic sea ice control on ocean circulation in present and glacial climates. Proc Natl Acad Sci U S A, **111**(24): 8753-8758.

Filippova A., Kienast M., Frank M. & Schneider R.R. 2016. Alkenone paleothermometry in the North Atlantic: A review and synthesis of surface sediment data and calibrations. Geochemistry, Geophysics, Geosystems, **17**(4): 1370-1382.

Fletcher M.S. & Moreno P.I. 2011. Zonally symmetric changes in the strength and position of the Southern Westerlies drove atmospheric CO2 variations over the past 14 k.y. Geology, **39**(5): 419-422.

Fogwill C.J., Turney C.S.M., Meissner K.J., Golledge N.R., Spence P., Roberts J.L., England M.H., Jones R.T. & Carter L. 2014. Testing the sensitivity of the East Antarctic Ice Sheet to Southern Ocean dynamics: past changes and future implications. Journal of Quaternary Science, **29**(1): 91-98.

Gersonde R., Abelmann A., Brathauer U., Becquey S., Bianchi C., Cortese G., Grobe H., Kuhn G., Niebler H.S., Segl M., Sieger R., Zielinski U. & Fütterer D.K. 2003. Last glacial sea surface temperatures and sea-ice extent in the Southern Ocean (Atlantic-Indian sector): A multiproxy approach. Paleoceanography, **18**(3): n/a-n/a.

Gersonde R., Crosta X., Abelmann A. & Armand L. 2005. Sea-surface temperature and sea ice distribution of the Southern Ocean at the EPILOG Last Glacial Maximum—a circum-Antarctic view based on siliceous microfossil records. Quaternary Science Reviews, **24**(7-9): 869-896.

643 Gersonde R. & Zielinski U. 2000. The reconstruction of late Quaternary Antarctic sea-ice distribution—
644 the use of diatoms as a proxy for sea-ice. Palaeogeography, Palaeoclimatology, Palaeoecology, **162**:
645 263-286.

646 Gille S.T. 2014. Meridional displacement of the Antarctic Circumpolar Current. Philos Trans A Math
647 Phys Eng Sci, **372**(2019): 20130273.

648 Govin A., Capron E., Tzedakis P.C., Verheyden S., Ghaleb B., Hillaire-Marcel C., St-Onge G., Stoner J.S.,
649 Bassinot F., Bazin L., Blunier T., Combourieu-Nebout N., El Ouahabi A., Genty D., Gersonde R., Jimenez-
650 Amat P., Landais A., Martrat B., Masson-Delmotte V., Parrenin F., Seidenkrantz M.S., Veres D.,
651 Waelbroeck C. & Zahn R. 2015. Sequence of events from the onset to the demise of the Last
652 Interglacial: Evaluating strengths and limitations of chronologies used in climatic archives. Quaternary
653 Science Reviews, **129**: 1-36.

654 Govin A., Michel E., Labeyrie L., Waelbroeck C., Dewilde F. & Jansen E. 2009. Evidence for northward
655 expansion of Antarctic Bottom Water mass in the Southern Ocean during the last glacial inception.
656 Paleoceanography, **24**(1): PA1202.

657 Haid V. & Timmermann R. 2013. Simulated heat flux and sea ice production at coastal polynyas in the
658 southwestern Weddell Sea. Journal of Geophysical Research: Oceans, **118**(5): 2640-2652.

659 Hall A. & Visbeck M. 2002. Synchronous Variability in the Southern Hemisphere Atmosphere, Sea Ice,
660 and Ocean Resulting from the Annular Mode. Journal of Climate, **15**: 3043-3057.

661 Hayes C.T., Martinez-Garcia A., Hasenfratz A.P., Jaccard S.L., Hodell D.A., Sigman D.M., Haug G.H. &
662 Anderson R.F. 2014. A stagnation event in the deep South Atlantic during the last interglacial period.
663 Science, **346**(6216): 1514-1517.

664 Hays J.D., Imbrie J. & Shackleton N.J. 1976. Variations in the Earth's Orbit: Pacemaker of the Ice Ages.
665 Science, **194**: 1121-1132.

666 Hellmer H.H., Kauker F., Timmermann R., Determann J. & Rae J. 2012. Twenty-first-century warming
667 of a large Antarctic ice-shelf cavity by a redirected coastal current. Nature, **485**(7397): 225-228.

668 Hillenbrand C.D., Smith J.A., Hodell D.A., Greaves M., Poole C.R., Kender S., Williams M., Andersen T.J.,
669 Jernas P.E., Elderfield H., Klages J.P., Roberts S.J., Gohl K., Larter R.D. & Kuhn G. 2017. West Antarctic
670 Ice Sheet retreat driven by Holocene warm water incursions. Nature, **547**(7661): 43-48.

671 Hobbs W.R., Massom R., Stammerjohn S., Reid P., Williams G. & Meier W. 2016. A review of recent
672 changes in Southern Ocean sea ice, their drivers and forcings. Global and Planetary Change, **143**: 228-
673 250.

674 Hoffman J.S., Clark P.U., Parnell A.C. & Feng H. 2017. Regional and global sea-surface temperatures
675 during the last interglaciation. Science, **355**: 276-279.

676 Holloway M.D., Sime L.C., Allen C.S., Hillenbrand C.-D., Bunch P., Wolff E. & Valdes P.J. 2017. The
677 spatial structure of the 128 ka Antarctic sea ice minimum. Geophysical Research Letters, **44**(21):
678 11129-11139.

679 Holloway M.D., Sime L.C., Singarayer J.S., Tindall J.C., Bunch P. & Valdes P.J. 2016. Antarctic last
680 interglacial isotope peak in response to sea ice retreat not ice-sheet collapse. Nature Communications,
681 **7:12293**.

682 Hutchings L., van der Lingen C.D., Shannon L.J., Crawford R.J.M., Verheye H.M.S., Bartholomae C.H.,
683 van der Plas A.K., Louw D., Kreiner A., Ostrowski M., Fidel Q., Barlow R.G., Lamont T., Coetzee J.,
684 Shillington F., Veitch J., Currie J.C. & Monteiro P.M.S. 2009. The Benguela Current: An ecosystem of
685 four components. Progress in Oceanography, **83**(1-4): 15-32.

686 Huybers P. & Denton G. 2008. Antarctic temperature at orbital timescales controlled by local summer
687 duration. Nature Geoscience, **1**(11): 787-792.

688 IPCC (2018). Global warming of 1.5°C. An IPCC Special Report on the impacts of global warming of
689 1.5°C above pre-industrial levels and related global greenhouse gas emission pathways, in the context
690 of strengthening the global response to the threat of climate change, sustainable development, and
691 efforts to eradicate poverty. Masson-Delmotte V., Zhai P., Portner H.O. et al. World Meteorological
692 Organisation, Geneva, Switzerland**:** 32.

693 Jenkins A., Dutrieux P., Jacobs S., Steig E., Gudmundsson H., Smith J. & Heywood K. 2016. Decadal
694 Ocean Forcing and Antarctic Ice Sheet Response: Lessons from the Amundsen Sea. Oceanography,
695 **29**(4): 106-117.

696 Kanfoush S.L., Hodell D.A., Charles C.D., Janecek T.R. & Rack F.R. 2002. Comparison of ice-rafted debris
697 and physical properties in ODP Site 1094 (South Atlantic) with the Vostok ice core over the last four
698 climatic cycles. Palaeogeography, Palaeoclimatology, Palaeoecology, **182**: 329-349.

699 King J. 2014. A resolution of the Antarctic paradox. Nature, **505**: 491-492.

700 Kopp R.E., Simons F.J., Mitrovica J.X., Maloof A.C. & Oppenheimer M. 2009. Probabilistic assessment
701 of sea level during the last interglacial stage. Nature, **462**(7275): 863-867.

702 Labeyrie L., Labracherie M., Gorfti N., Pichon J.J., Vautravers M., Arnold M., Duplessy J.-C., Paterne M.,
703 Michel E., Duprat J., Caralp M. & Turon J.-L. 1996. Hydrographic changes of the Southern Ocean
704 (southeast Indian Sector) Over the last 230 kyr. Paleoceanography, **11**(1): 57-76.

705 Lisiecki L.E. & Raymo M.E. 2005. A Pliocene-Pleistocene stack of 57 globally distributed benthic δ18O
706 records. Paleoceanography, **20**(1): PA1003.

707 Liu J. & Curry J.A. 2010. Accelerated warming of the Southern Ocean and its impacts on the
708 hydrological cycle and sea ice. Proc Natl Acad Sci U S A, **107**(34): 14987-14992.

709 Maheshwari M., Singh R.K., Oza S.R. & Kumar R. 2013. An Investigation of the Southern Ocean Surface
710 Temperature Variability Using Long-Term Optimum Interpolation SST Data. ISRN Oceanography, **2013**:
711 1-9.

712 Marino G., Rohling E.J., Rodriguez-Sanz L., Grant K.M., Heslop D., Roberts A.P., Stanford J.D. & Yu J.
713 2015. Bipolar seesaw control on last interglacial sea level. Nature, **522**(7555): 197-201.

714 Martinson D.G., Pisias N.G., Hays J.D., Imbrie J., Moore T.C. & Shackleton N.J. 1987. Age Dating and
715 the Orbital Theory of the Ice Ages: Development of a High-Resolution 0 to 300,000-Year
716 Chronostratigraphy. Quaternary Research, **27**: 1-29.

717 Masson-Delmotte V., Buiron D., Ekaykin A., Frezzotti M., Gallée H., Jouzel J., Krinner G., Landais A.,
718 Motoyama H., Oerter H., Pol K., Pollard D., Ritz C., Schlosser E., Sime L.C., Sodemann H., Stenni B.,
719 Uemura R. & Vimeux F. 2011. A comparison of the present and last interglacial periods in six Antarctic
720 ice cores. Climate of the Past, **7**(2): 397-423.

721 Mazloff M.R. 2012. On the Sensitivity of the Drake Passage Transport to Air–Sea Momentum Flux.
722 Journal of Climate, **25**(7): 2279-2290.

723 Meinen C.S., Luther D.S., Watts D.R., Chave A.D. & Tracey K.L. 2003. Mean stream coordinates
724 structure of the Subantarctic Front: Temperature, salinity, and absolute velocity. Journal of
725 Geophysical Research, **108**(C8): 3263.

726 Moore J.K., Abbott M.R. & Richman J.G. 1999. Location and dynamics of the Antarctic Polar Front from
727 satellite sea surface temperature data. Journal of Geophysical Research, **104**(C2): 3059-3073.

728 Mulitza S., Arz H.W., Kemle-von Mucke S., Moos C., Niebler H.-S., Patzold J. & Segl M. (1999).
729 Foraminifera isotopes of sediment core PS1768-8. PANGAEA.

730 Neil H.L., Carter L. & Morris M.Y. 2004. Thermal isolation of Campbell Plateau, New Zealand, by the
731 Antarctic Circumpolar Current over the past 130 kyr. Paleoceanography, **19**(4): n/a-n/a.

732 Nelson C.S., Cooke P.J., Hendy C.H. & Cuthbertson A.M. 1993. Oceanographic and climatic changes
733 over the past 160,000 years at Deep Sea Drilling Project Site 594 off Southeastern New Zealand,
734 Southwest Pacific Ocean. Paleoceanography, **8**(4): 435-458.

735 Niebler H.-S. 1995. Reconstruction of paleo-environmental parameters using stable isotopes and
736 faunal assemblages of planktonic foraminifera in the South Atlantic Ocean. Reports on Polar Research,
737 **167**: 1-198.

738 Orsi A.H., Whitworth III T. & Nowlin Jr W.D. 1995. On the meridional extent and fronts of the Antarctic
739 Circumpolar Current. Deep Sea Research I, **42**(5): 641-673.

740 Otto-Bliesner B.L., Rosenbloom N., Stone E.J., McKay N.P., Lunt D.J., Brady E.C. & Overpeck J.T. 2013.
741 How warm was the last interglacial? New model-data comparisons. Philos Trans A Math Phys Eng Sci,
742 **371**(2001): 20130097.

743 Pahnke K., Zahn R., Elderfield H. & Schulz M. 2003. 340,000-Year Centennial-Scale Marine Record of
744 Southern Hemisphere Climatic Oscillation. Science, **301**: 948-952.

745 Paillard D., Labeyrie L. & Yiou P. 1996. Macintosh program performs time-series analysis. Eos, **77**: 379.

746 Parkinson C.L. 2019. A 40-y record reveals gradual Antarctic sea ice increases followed by decreases
747 at rates far exceeding the rates seen in the Arctic. Proc Natl Acad Sci U S A, **116**(29): 14414-14423.

748 Parrenin F., Masson-Delmotte V., Kohler P., Raynaud D., Paillard D., Schwander J., Barbante C., Landais
749 A., Wegner A. & Jouzel J. (2013). Synchronisation of the LR04 stack with EDC isotopic variations on the
750 EDC3 age scale. PANGAEA.

751 Pelejero C., Calvo E., Barrows T.T., Logan G.A. & De Deckker P. 2006. South Tasman Sea alkenone
752 palaeothermometry over the last four glacial/interglacial cycles. Marine Geology, **230**(1-2): 73-86.

753 Pichon J.J., Labeyrie L.D., Bareille G., Labracherie M., Duprat J. & Jouzel J. 1992. Surface Water
754 Temperature Changes in the High Latitudes of the Southern Hemisphere over the Last Glacial-
755 Interglacial Cycle. Paleoceanography, **7**(3): 289-318.

756 Pollard D. & DeConto R.M. 2009. Modelling West Antarctic ice sheet growth and collapse through the
757 past five million years. Nature, **458**(7236): 329-332.

Pugh R.S., McCave I.N., Hillenbrand C.D. & Kuhn G. 2009. Circum-Antarctic age modelling of Quaternary marine cores under the Antarctic Circumpolar Current: Ice-core dust–magnetic correlation. Earth and Planetary Science Letters, **284**(1-2): 113-123.

Purich A., England M.H., Cai W., Chikamoto Y., Timmermann A., Fyfe J.C., Frankcombe L., Meehl G.A. & Arblaster J.M. 2016. Tropical Pacific SST Drivers of Recent Antarctic Sea Ice Trends. Journal of Climate, **29**(24): 8931-8948.

Rignot E., Mouginot J., Scheuchl B., van den Broeke M., van Wessem M.J. & Morlighem M. 2019. Four decades of Antarctic Ice Sheet mass balance from 1979-2017. Proc Natl Acad Sci U S A, **116**(4): 1095-1103.

Russell J.L., Dixon K.W., Gnanadesikan A., Stouffer R.J. & Toggweiler J.R. 2006. The Southern Hemisphere Westerlies in a Warming World: Propping Open the Door to the Deep Ocean. Journal of Climate, **19**: 6382-6390.

Saunders K.M., Kamenik C., Hodgson D.A., Hunziker S., Siffert L., Fischer D., Fujak M., Gibson J.A.E. & Grosjean M. 2012. Late Holocene changes in precipitation in northwest Tasmania and their potential links to shifts in the Southern Hemisphere westerly winds. Global and Planetary Change, **92-93**: 82-91.

Scherer R.P. 1994. A new method for the determination of absolute abundance of diatoms and other silt-sized sedimentary particles. Journal of Paleolimnology, **12**(2): 171-179.

Schmidtko S., Heywood K.J., Thompson A.F. & Aoki S. 2014. Multidecadal warming of Antarctic waters. Science, **346**(6214): 1227-1231.

Schneider Mor A., Yam R., Bianchi C., Kunz-Pirrung M., Gersonde R. & Shemesh A. 2012. Variable sequence of events during the past seven terminations in two deep-sea cores from the Southern Ocean. Quaternary Research, **77**(02): 317-325.

Shepherd A., Ivins E., Rignot E., Smith B., van den Broeke M., Velicogna I., Whitehouse P., Briggs K., Joughin I., Krinner G., Nowicki S., Payne T., Scambos T., Schlegel N., A G., Agosta C., Ahlstrom A., Babonis G., Barletta V., Blazquez A., Bonin J., Csatho B., Cullather R., Felikson D., Fettweis X., Forsberg R., Gallée H., Gardner A., Gilbert L., Groh A., et al. 2018. Mass balance of the Antarctic Ice Sheet from 1992 to 2017. Nature, **558**(7709): 219-222.

Sikes E.L., Howard W.R., Neil H.A. & K. V.J. 2002. Glacial-interglacial sea surface temperature changes across the subtropical front east of New Zealand based on alkenone unsaturation ratios and foraminiferal assemblages. Paleoceanography, **17**(2): 1-13.

Sokolov S. & Rintoul S.R. 2009. Circumpolar structure and distribution of the Antarctic Circumpolar Current fronts: 1. Mean circumpolar paths. Journal of Geophysical Research, **114**: C11018.

Spence P., Holmes R.M., Hogg A.M., Griffies S.M., Stewart K.D. & England M.H. 2017. Localized rapid warming of West Antarctic subsurface waters by remote winds. Nature Climate Change, **7**(8): 595-603.

Stammerjohn S.E., Martinson D.G., Smith R.C., Yuan X. & Rind D. 2008. Trends in Antarctic annual sea ice retreat and advance and their relation to El Niño–Southern Oscillation and Southern Annular Mode variability. Journal of Geophysical Research, **113**(C3): C03S90.

Stocker T.F. & Johnsen S.J. 2003. A minimum thermodynamic model for the bipolar seesaw. Paleoceanography, **18**(4): n/a-n/a.

798 Stone E.J., Capron E., Lunt D.J., Payne A.J., Singarayer J.S., Valdes P.J. & Wolff E.W. 2016. Impact of
799 meltwater on high-latitude early Last Interglacial climate. Climate of the Past, **12**(9): 1919-1932.

800 Tim N., Zorita E., Schwarzkopf F.U., Rühs S., Emeis K.C. & Biastoch A. 2018. The impact of Agulhas
801 leakage on the central water masses in the Benguela upwelling system from a high-resolution ocean
802 simulation. Journal of Geophysical Research: Oceans, **123**: 9416-9428.

803 Trathan P.N., Brandon M.A., Murphy E.J. & E. T.S. 2000. Transport and structure within the Antarctic
804 Circumpolar Current to the north of South Georgia. Geophysical Research Letters, **27**(12): 1727-1730.

805 Vaughan D.G., Comiso J.C., Allison I., Carrasco J., Kaser G., Kwok R., Mote P., Murray T., Paul F., Ren J.,
806 Rignot E., Solomina O., Steffen K. & Zhang T. (2013). Observations: Cryosphere. Climate Change 2013:
807 The Physical Science Basis. Contribution of Working Group I to the Fifth Assessment Report of the
808 Intergovernmental Panel on Climate Change. Stocker T.F., Qin D., Plattner G.-K. et al. Cambridge,
809 United Kingdom and New York, NY, USA, Cambridge University Press**:** 317–382.

810 Waelbroeck C., Paul A., Kucera M., Rosell-Melé A., Weinelt M., Schneider R., Mix A.C., Abelmann A.,
811 Armand L., Bard E., Barker S., Barrows T.T., Benway H., Cacho I., Chen M.T., Cortijo E., Crosta X., de
812 Vernal A., Dokken T., Duprat J., Elderfield H., Eynaud F., Gersonde R., Hayes A., Henry M., Hillaire-
813 Marcel C., Huang C.C., Jansen E., Juggins S., Kallel N., et al. 2009. Constraints on the magnitude and
814 patterns of ocean cooling at the Last Glacial Maximum. Nature Geoscience, **2**(2): 127-132.

815 Wang Z. 2013. On the response of Southern Hemisphere subpolar gyres to climate change in coupled
816 climate models. Journal of Geophysical Research: Oceans, **118**(3): 1070-1086.

817 Wolff E.W., Fischer H., Fundel F., Ruth U., Twarloh B., Littot G.C., Mulvaney R., Rothlisberger R., de
818 Angelis M., Boutron C.F., Hansson M., Jonsell U., Hutterli M.A., Lambert F., Kaufmann P., Stauffer B.,
819 Stocker T.F., Steffensen J.P., Bigler M., Siggaard-Andersen M.L., Udisti R., Becagli S., Castellano E.,
820 Severi M., Wagenbach D., Barbante C., Gabrielli P. & Gaspari V. 2006. Southern Ocean sea-ice extent,
821 productivity and iron flux over the past eight glacial cycles. Nature, **440**(7083): 491-496.

822 Xiao W., Esper O. & Gersonde R. 2016. Last Glacial - Holocene climate variability in the Atlantic sector
823 of the Southern Ocean. Quaternary Science Reviews, **135**: 115-137.

824 Zielinski U., Gersonde R., Sieger R. & Futterer D. 1998. Quaternary surface water temperature
825 estimations: Calibration of a diatom transfer function for the Southern Ocean. Paleoceanography,
826 **13**(4): 365-383.

Supplemental Material: Analysing the timing of peak warming and minimum winter sea-ice extent in the Southern Ocean during MIS 5e

M. Chadwick[1,2]; C.S. Allen[1]; L.C. Sime[1] & C.-D. Hillenbrand[1]

[1.] *British Antarctic Survey, High Cross, Madingley Road, Cambridge, CB3 0ET, UK*

[2.] *Ocean and Earth Science, National Oceanography Centre, University of Southampton Waterfront Campus, European Way, Southampton, SO14 3ZH, UK*

Core	Latitude (°S), Longitude (°E)	Oceanographic Position	Modern SST (°C) (*SSST)	Modern Sea Ice	Chronology for MIS 5e	SST Proxy for MIS 5e	Sample Resolution (ka)
Atlantic sector							
PS2489-2	42.87, 8.97	SAZ	10* (Becquey & Gersonde 2003)	1	Correlating benthic $\delta^{18}O$ with SPECMAP (Becquey & Gersonde 2003)	Planktonic foraminifera transfer function (Becquey & Gersonde 2003)	1.2-3
PS1778-5	49.01, -12.7	PFZ	4.38* (Waelbroeck et al. 2009)	1	*C. davisiana* stratigraphy (Brathauer & Abelmann 1999)	Radiolarian transfer function (Brathauer & Abelmann 1999)	1.2-5
ODP 1093	49.98, 5.87	AZ	3.6* (Schneider Mor et al. 2012)	1	Correlating SSST, *N.pachyderma* $\delta^{18}O$ and Magnetic Susceptibility with δD and dust in Antarctic ice cores (Schneider Mor et al. 2012)	Diatom transfer function (Schneider Mor et al. 2012)	1
PS1768-8	52.59, 4.48	AZ	2.5* (Waelbroeck et al. 2009)	1	$^{230}Th_{ex}$ record (Frank et al. 1996)	Diatom transfer function (Zielinski et al. 1998)	1-4
PS2102-2	53.07, -4.99	AZ	1.84* (Waelbroeck et al. 2009)	1	Correlating *N.pachyderma* $\delta^{18}O$ with orbital variations and combined with diatom biofluctuation zones (Bianchi & Gersonde 2002)	Diatom transfer function (Bianchi & Gersonde 2002)	0.6-3
ODP 1094	53.18, 5.13	AZ	2.2* (Capron et al. 2014)	1	Correlating SSST, *N.pachyderma* $\delta^{18}O$ and Magnetic Susceptibility with δD and dust in Antarctic ice cores (Schneider Mor et al. 2012) Correlating *N.pachyderma* $\delta^{18}O$ with orbital variations and combined with diatom	Diatom transfer function (Bianchi & Gersonde 2002, Schneider Mor et al. 2012)	0.07-1.4 1

Core	Latitude (°S), Longitude (°E)	Oceanographic Position	Modern SST (°C) (*SSST)	Modern Sea Ice	Chronology for MIS 5e	SST Proxy for MIS 5e	Sample Resolution (ka)
					biofluctuation zones (Bianchi & Gersonde 2002)		
PS2276-4	54.64, -23.57	AZ	1.71* (Waelbroeck et al. 2009)	2	Diatom biofluctuation zones (Bianchi & Gersonde 2002)	Diatom transfer function (Bianchi & Gersonde 2002)	0.8-1.6
PS2305-6	58.72, -33.04	AZ	0.78* (Waelbroeck et al. 2009)	3	Diatom biofluctuation zones (Bianchi & Gersonde 2002)	Diatom transfer function (Bianchi & Gersonde 2002)	0.5-4.1
Indian sector							
RC11-120	43.52, 79.87	SAZ	11.43* (Waelbroeck et al. 2009)	1	Orbital tuning of benthic $\delta^{18}O$ (Martinson et al. 1987)	Radiolarian transfer function (Hays et al. 1976)	1.3-2.5
MD97-2106	45.15, 146.29	N of STF	12.58 (Cortese et al. 2013)	1	Correlating benthic $\delta^{18}O$ with LR04 (Cortese et al. 2013)	Planktonic foraminifera transfer function (Cortese et al. 2013)	1.2-1.6
MD88-770	46.02, 96.45	SAZ	8.1* (Govin et al. 2009)	1	Correlating benthic $\delta^{18}O$ with chronostratigraphy of core MD95-2042 on GISP timescale (Barrows et al. 2007)	Planktonic foraminifera transfer function (Barrows et al. 2007)	0.1-0.5
MD02-2488	46.48, 88.02	SAZ	9.1* (Govin et al. 2009)	1	Correlating SSST record to Deuterium record from EPICA Dome C ice core (Govin et al. 2009)	Planktonic foraminifera transfer function (Govin et al. 2009)	1-2
MD97-2108	48.5, 149.11	SAZ	9.49 (Cortese et al. 2013)	1	Correlating benthic $\delta^{18}O$ with LR04 (Cortese et al. 2013)	Planktonic foraminifera transfer function (Cortese et al. 2013)	2.8-2.9
MD84-551	55, 73.33	AZ	2.49* (Waelbroeck et al. 2009)	1	Correlating benthic $\delta^{18}O$ and $\delta^{`13}C$ and SST to core MD84-527 on SPECMAP time scale (Pichon et al. 1992)	Diatom transfer function (Pichon et al. 1992)	0.27-0.66
PS2603-3	58.99. 37.63	AZ	1.82* (Waelbroeck et al. 2009)	2	Diatom biofluctuation zones (Bianchi & Gersonde 2002)	Diatom transfer function (Bianchi & Gersonde 2002)	0.9-1.9
Pacific sector							
DSDP 593	40.51, 167.67	N of STF	15.61 (Cortese et al. 2013)	1	Correlating benthic $\delta^{18}O$ with LR04 (Cortese et al. 2013)	Planktonic foraminifera transfer function (Cortese et al. 2013)	3.2-9.7

Core	Latitude (°S), Longitude (°E)	Oceanographic Position	Modern SST (°C) (*SSST)	Modern Sea Ice	Chronology for MIS 5e	SST Proxy for MIS 5e	Sample Resolution (ka)
ODP 1123	41.79, -171.5	N of STF	14.94 (Cortese et al. 2013)	1	Correlating benthic $\delta^{18}O$ with LR04 (Cortese et al. 2013)	Planktonic foraminifera transfer function (Cortese et al. 2013)	2.4-3.1
SO136-003	42.3, 169.88	N of STF	15.4 (Pelejero et al. 2006) 15.55 (Cortese et al. 2013)	1	Correlating planktonic $\delta^{18}O$ to SPECMAP (Pelejero et al. 2006) Correlating benthic $\delta^{18}O$ with chronostratigraphy of core MD95-2042 on GISP timescale (Barrows et al. 2007) Correlating benthic $\delta^{18}O$ with LR04 (Cortese et al. 2013)	Alkenone based $U^{K'}_{37}$ (Pelejero et al. 2006) Planktonic foraminiferal transfer functions (Barrows et al. 2007) Planktonic foraminifera transfer function (Cortese et al. 2013)	0.5-3 0.5-4 0.8-4.4
MD06-2986	43.45, 167.9	N of STF	14.93 (Cortese et al. 2013)	1	Correlating benthic $\delta^{18}O$ with LR04 (Cortese et al. 2013)	Planktonic foraminifera transfer function (Cortese et al. 2013)	1.8-3.9
DSDP 594	45.52, 174.95	SAZ	10.41 (Cortese et al. 2013)	1	Correlating benthic $\delta^{18}O$ with LR04 (Cortese et al. 2013) Correlating planktonic $\delta^{18}O$ with core MD95-2042 on GISP timescale (Barrows et al. 2007)	Planktonic foraminifera transfer function (Cortese et al. 2013) Planktonic foraminifera transfer functions (Barrows et al. 2007)	0.1-2.1 0.5-16
MD97-2120	45.54, 174.93	SAZ	11.8 (Pahnke et al. 2003)	1	Correlating SST to the δD in the Vostok ice core (Pahnke et al. 2003)	Mg/Ca composition of *Gg. bulloides* (Pahnke et al. 2003)	0.5-1
Y9	48.24, 177.34	SAZ	8.82 (Cortese et al. 2013)	1	Correlating benthic $\delta^{18}O$ with LR04 (Cortese et al. 2013)	Planktonic foraminifera transfer function (Cortese et al. 2013)	1.9-2.7
MD97-2109	50.63, 169.38	SAZ	9.05 (Cortese et al. 2013)	1	Correlating benthic $\delta^{18}O$ with LR04 (Cortese et al. 2013)	Planktonic foraminifera transfer function (Cortese et al. 2013)	1.9-2.9
SO136-111	56.67, 160.23	PFZ	5.54* (Waelbroeck et al. 2009)	1	Correlating benthic $\delta^{18}O$ to SPECMAP (Crosta et al. 2004)	Diatom transfer function (Crosta et al. 2004)	0.5-1.7
PS58/271-1	61.24, -116.05	PFZ	3.05* (Waelbroeck et al. 2009)	1	Correlating physical parameters, XRF elemental concentrations and diatom assemblages with EDC ice core record and diatom biostratigraphy (Esper & Gersonde 2014a)	Diatom transfer function (Esper & Gersonde 2014b)	0.1-0.2

Supplementary Table 1: Details for the cores analysed as part of this study. Cores are ordered by latitude within the three Southern Ocean (SO) sectors (Atlantic-Indian-Pacific). The position of the cores relative to the modern SO fronts is given along with the modern sea-surface temperature (SST) (asterisks indicate summer SST [SSST] rather than mean annual SST) and the present sea ice conditions. For the sea ice conditions (Gersonde et al. 2003, Gersonde et al. 2005): 1 – core is located north of the maximum winter sea ice limit (FCC <1 %), 2 – core is located north of the mean and south of the maximum winter sea ice limit (FCC =1-3 %), 3 – core is located at and south of the mean winter sea ice limit (FCC >3%) (limit of maximum sea ice extent is based on ~15-20 % concentration and limit of mean sea-ice extent is based on 50-80% concentration for September (winter) and February (summer) for the years 1982 to 2002). The chronological method applied to a core and the proxy method used to determine MIS 5e SSTs together with the sample resolution and the source data references are also given. The chronological method gives the details of the published chronologies before standardisation onto the LR04 benthic stack. AZ: Antarctic Zone, PFZ: Polar Frontal Zone, SAZ: Subantarctic Zone.

833

	Age of MIS 5e Sea Ice Min (ka)	MIS 5e Minimum Sea Ice Conditions	Age of MIS 5e SST peak (ka)	Error on MIS 5e SST peak age (ka)	MIS 5e Peak SST (°C) (*SSST)	MIS 5e Oceanographic Setting	References for MIS 5e Conditions
Atlantic sector							
PS2489-2	-	-	125.14	+0.86, -0.58	11.8*	SAZ	(Becquey & Gersonde 2003)
PS1778-5	-	-	124.1	+2.57, -0.60	6.8*	SAZ	(Brathauer & Abelmann 1999)
ODP 1093	125.96 ± 1.23	1	125.82	±0.3	5.0*	PFZ	(Schneider Mor et al. 2012)
PS1768-8	123.4 ± 1.66	1	124.22	±0.83	3.9*	PFZ	(Zielinski et al. 1998)
PS2102-2	127.13 ± 0.69	1	126.68	±0.5	3.8*	PFZ	(Bianchi & Gersonde 2002)
ODP 1094	127.14 ± 1.32	1	127.57	+0.05, -0.03	4.7*	PFZ	(Bianchi & Gersonde 2002)
	126.68 ± 1.61	1	127.32	±0.04	4.8*	PFZ	(Schneider Mor et al. 2012)
PS2276-4	127.99 ± 0.5	1	127.25	±0.35	3.1*	PFZ	(Bianchi & Gersonde 2002)
PS2305-6	128.58 ± 1.05	1	127.19	+0.70, -0.65	1.3*	AZ	(Bianchi & Gersonde 2002)
Indian sector							
RC11-120	-	-	130.08	+0.69, -0.66	13.5*	N of STF	(Martinson et al. 1987)
MD97-2106	-	-	129.76	±0.63	16.1	N of STF	(Cortese et al. 2013)
MD88-770	-	-	126	±0.25	11.1	SAZ	(Barrows et al. 2007)
MD02-2488	-	-	127.2	+0.14, -0.28	13.3*	N of STF	(Govin et al. 2009)
MD97-2108	-	-	127.8	+1.40, -1.45	14.4	N of STF	(Cortese et al. 2013)

	Age of MIS 5e Sea Ice Min (ka)	MIS 5e Minimum Sea Ice Conditions	Age of MIS 5e SST peak (ka)	Error on MIS 5e SST peak age (ka)	MIS 5e Peak SST (°C) (*SSST)	MIS 5e Oceanographic Setting	References for MIS 5e Conditions
MD84-551	-	-	128.37	±0.64	6.1*	PFZ	(Pichon et al. 1992)
PS2603-3	124.47 ± 3	1	127.34	+0.75, -0.70	3.8*	PFZ	(Bianchi & Gersonde 2002)
Pacific sector							
DSDP 593	-	-	111.04	+1.61, -4.83	15.1	N of STF	(Cortese et al. 2013)
ODP 1123	-	-	118.8	±1.4	17.4	N of STF	(Cortese et al. 2013)
SO136-003	-	-	132	±0.3	15.4	N of STF	(Barrows et al. 2007)
	-	-	131.7	±0.3	15.6	N of STF	(Cortese et al. 2013)
	-	-	131.43	±0.3	19.0	N of STF	(Pelejero et al. 2006)
MD06-2986	-	-	126.1	+1.1, -0.9	16.4	N of STF	(Cortese et al. 2013)
DSDP 594	-	-	123.1	+0.5, -0.9	15.2	N of STF	(Cortese et al. 2013)
	-	-	131	±0.5	15.6	N of STF	(Barrows et al. 2007)
MD97-2120	-	-	126.24	±0.75	16.1	N of STF	(Pahnke et al. 2003)
Y9	-	-	121.8	±1.25	12.3	SAZ	(Cortese et al. 2013)
MD97-2109	-	-	122.4	+1.40, -1.45	11.6	SAZ	(Cortese et al. 2013)
SO136-111	125.45 ± 0.73	1	124.72	+0.29, -0.73	6.1*	PFZ	(Crosta et al. 2004)
PS58/271-1	-	-	124.6	+0.11, -0.10	3.1*	PFZ	(Esper & Gersonde 2014b, a)

834

Supplementary Table 2: Published ages and values of MIS 5e peak SSTs with associated errors from the sample resolution (+ indicates younger ages, - indicates older ages). Ages for the MIS 5e minimum in winter sea ice extent (WSIE) are given as the centre age of an MIS 5e interval with either FCC <1 % or FCC =0 % (for a core with an MIS 5e interval barren of sea-ice diatoms), with the errors indicating the duration of this interval. The peak MIS 5e SSTs are also given alongside the inferred oceanographic setting, assuming that SSTs at fronts during MIS 5e were similar to those at the modern SO fronts. Cores are listed in the same order as in Supplementary Table 1. All ages are given using the original chronologies before conversion onto the LR04 benthic stack age model. AZ: Antarctic Zone, PFZ: Polar Frontal Zone, SAZ: Subantarctic Zone, STF: Subtropical Front.

835

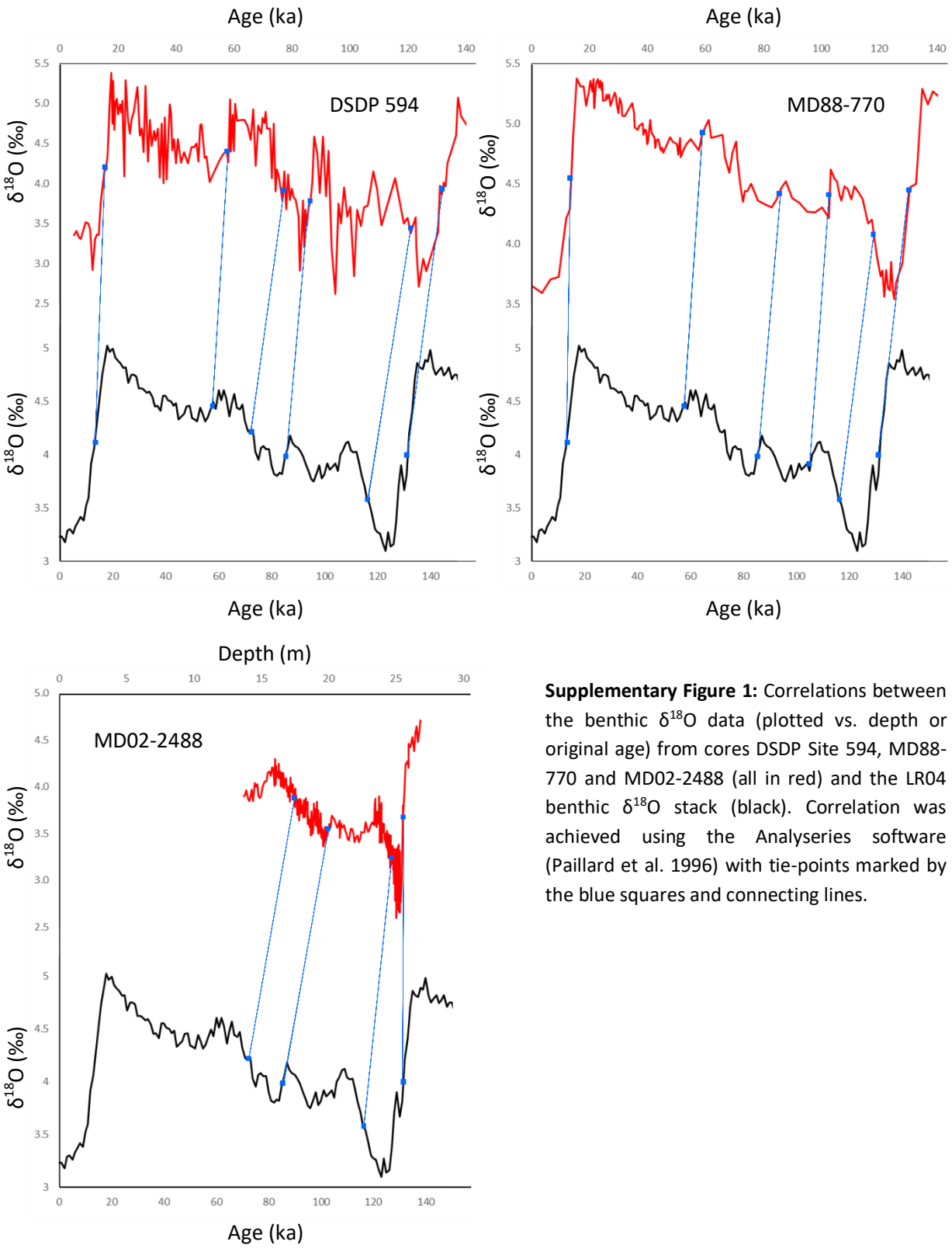

Supplementary Figure 1: Correlations between the benthic $\delta^{18}O$ data (plotted vs. depth or original age) from cores DSDP Site 594, MD88-770 and MD02-2488 (all in red) and the LR04 benthic $\delta^{18}O$ stack (black). Correlation was achieved using the Analyseries software (Paillard et al. 1996) with tie-points marked by the blue squares and connecting lines.

836

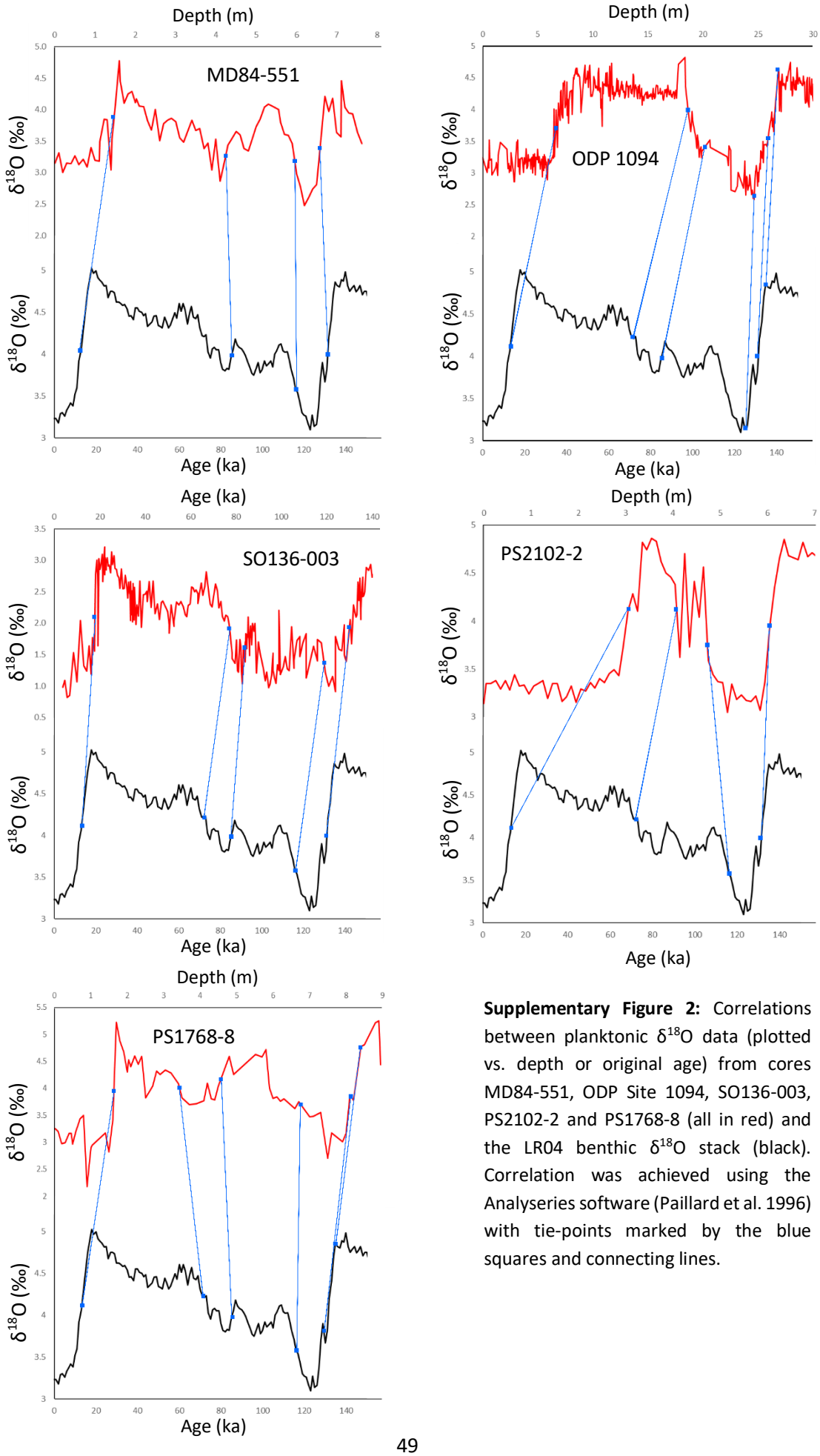

Supplementary Figure 2: Correlations between planktonic $\delta^{18}O$ data (plotted vs. depth or original age) from cores MD84-551, ODP Site 1094, SO136-003, PS2102-2 and PS1768-8 (all in red) and the LR04 benthic $\delta^{18}O$ stack (black). Correlation was achieved using the Analyseries software (Paillard et al. 1996) with tie-points marked by the blue squares and connecting lines.

Tie-point selection

The tie-points used to correlate $\delta^{18}O$ data from core records to the LR04 stack were selected as the midpoints of $\delta^{18}O$ shifts which mark MIS stage or sub-stage boundaries. The boundaries used as tie-points for each of the nine correlated cores are listed in Supplementary Table 3 with the age assignments for the MIS 5 sub-stages following (Govin et al. 2009). For each core a minimum of 4 tie-points were selected with a maximum of 6 imposed by the Analyseries software. All nine cores have a tie-point at the midpoint of Termination II and, with the exception of MD02-2488, Termination I. The other prominent boundaries used as tie-points in most of the core records were MIS 4-5a, MIS 5a-5b and MIS 5d-5e. Only core ODP Site 1094 and PS1768-8 have tie-points that do not mark stage or sub-stage boundaries. Both cores have a tie-point at the initiation of Termination II which was added to help with graphical alignment of the records but does not influence the age model for the interval of interest in this study. ODP Site 1094 also has a tie-point at the $\delta^{18}O$ minimum during MIS 5e which was added to counter the poor sample resolution during MIS 5d-5b. Without this additional tie-point there would be no age constraints for ODP Site 1094 between the mid-point of Termination II and the MIS 5a-5b boundary. The depth/"age" and age values for the tiepoints are presented in Chadwick (2019a).

	Termination I	*MIS 3-4*	*MIS 4-5a*	*MIS 5a-5b*	*MIS 5c-5d*	*MIS 5d-5e*	*Termination II*
DSDP 594	X	X	X	X		X	X
MD88-770	X	X		X	X	X	X
MD02-2488			X	X		X	X
MD84-551	X			X		X	X
ODP 1094	X		X	X			X
SO136-003	X		X	X		X	X
PS1768-8	X		X	X		X	X
PS2102-2	X		X			X	X
MD97-2120	X		X	X	X	X	X

Supplementary Table 3: The MIS stage and sub-stage boundaries used as tie-points in each of the nine core records to correlate their $\delta^{18}O$ values to the LR04 stack. **X** marks where a stage or sub-stage boundary has been used as a tie-point for that record. Only core ODP Site 1094 and PS1768-8 have tie-points that are not (sub-)stage boundaries and thus are not listed here.

References

Barrows T.T., Juggins S., De Deckker P., Calvo E. & Pelejero C. 2007. Long-term sea surface temperature and climate change in the Australian-New Zealand region. Paleoceanography, 22(2): PA2215.

Becquey S. & Gersonde R. 2003. A 0.55-Ma paleotemperature record from the Subantarctic zone: Implications for Antarctic Circumpolar Current development. Paleoceanography, 18(1): 1014-1028.

Bianchi C. & Gersonde R. 2002. The Southern Ocean surface between Marine Isotope Stages 6 and 5d: Shape and timing of climate changes. Palaeogeography, Palaeoclimatology, Palaeoecology, 187: 151-177.

Brathauer U. & Abelmann A. 1999. Late Quaternary variations in sea surface temperatures and their relationship to orbital forcing recorded in the Southern Ocean (Atlantic sector). Paleoceanography, 14(2): 135-148.

Capron E., Govin A., Stone E.J., Masson-Delmotte V., Mulitza S., Otto-Bliesner B., Rasmussen T.L., Sime L.C., Waelbroeck C. & Wolff E.W. 2014. Temporal and spatial structure of multi-millennial temperature changes at high latitudes during the Last Interglacial. Quaternary Science Reviews, 103: 116-133.

Chadwick M. (2019). Age-model tiepoints for cores DSDP 594, MD88-770, MD02-2488, MD84-551, ODP site 1094, SO136-003, PS1768-8, PS2102-2 and MD97-2120. Mendeley Data.

Cortese G., Dunbar G.B., Carter L., Scott G., Bostock H., Bowen M., Crundwell M., Hayward B.W., Howard W., Martínez J.I., Moy A., Neil H., Sabaa A. & Sturm A. 2013. Southwest Pacific Ocean response to a warmer world: Insights from Marine Isotope Stage 5e. Paleoceanography, 28(3): 585-598.

Crosta X., Sturm A., Armand L. & Pichon J.-J. 2004. Late Quaternary sea ice history in the Indian sector of the Southern Ocean as recorded by diatom assemblages. Marine Micropaleontology, 50(3-4): 209-223.

Esper O. & Gersonde R. 2014a. New tools for the reconstruction of Pleistocene Antarctic sea ice. Palaeogeography, Palaeoclimatology, Palaeoecology, 399: 260-283.

Esper O. & Gersonde R. 2014b. Quaternary surface water temperature estimations: New diatom transfer functions for the Southern Ocean. Palaeogeography, Palaeoclimatology, Palaeoecology, 414: 1-19.

Frank M., Gersonde R., Rutgers van der Loeff M., Kuhn G. & Mangini A. 1996. Late Quaternary sediment dating and quantification of lateral sediment redistribution applying 230Thex: a study from the eastern Atlantic sector of the Southern Ocean. Geol Rundsch, 85: 544-566.

Gersonde R., Abelmann A., Brathauer U., Becquey S., Bianchi C., Cortese G., Grobe H., Kuhn G., Niebler H.S., Segl M., Sieger R., Zielinski U. & Fütterer D.K. 2003. Last glacial sea surface temperatures and sea-ice extent in the Southern Ocean (Atlantic-Indian sector): A multiproxy approach. Paleoceanography, 18(3): n/a-n/a.

Gersonde R., Crosta X., Abelmann A. & Armand L. 2005. Sea-surface temperature and sea ice distribution of the Southern Ocean at the EPILOG Last Glacial Maximum—a circum-Antarctic view based on siliceous microfossil records. Quaternary Science Reviews, 24(7-9): 869-896.

Govin A., Michel E., Labeyrie L., Waelbroeck C., Dewilde F. & Jansen E. 2009. Evidence for northward expansion of Antarctic Bottom Water mass in the Southern Ocean during the last glacial inception. Paleoceanography, 24(1): PA1202.

Hays J.D., Imbrie J. & Shackleton N.J. 1976. Variations in the Earth's Orbit: Pacemaker of the Ice Ages. Science, 194: 1121-1132.

Martinson D.G., Pisias N.G., Hays J.D., Imbrie J., Moore T.C. & Shackleton N.J. 1987. Age Dating and the Orbital Theory of the Ice Ages: Development of a High-Resolution 0 to 300,000-Year Chronostratigraphy. Quaternary Research, 27: 1-29.

Pahnke K., Zahn R., Elderfield H. & Schulz M. 2003. 340,000-Year Centennial-Scale Marine Record of Southern Hemisphere Climatic Oscillation. Science, 301: 948-952.

Paillard D., Labeyrie L. & Yiou P. 1996. Macintosh program performs time-series analysis. Eos, 77: 379.

Pelejero C., Calvo E., Barrows T.T., Logan G.A. & De Deckker P. 2006. South Tasman Sea alkenone palaeothermometry over the last four glacial/interglacial cycles. Marine Geology, 230(1-2): 73-86.

Pichon J.J., Labeyrie L.D., Bareille G., Labracherie M., Duprat J. & Jouzel J. 1992. Surface Water Temperature Changes in the High Latitudes of the Southern Hemisphere over the Last Glacial-Interglacial Cycle. Paleoceanography, 7(3): 289-318.

905 Schneider Mor A., Yam R., Bianchi C., Kunz-Pirrung M., Gersonde R. & Shemesh A. 2012. Variable
906 sequence of events during the past seven terminations in two deep-sea cores from the Southern
907 Ocean. Quaternary Research, 77(02): 317-325.

908 Waelbroeck C., Paul A., Kucera M., Rosell-Melé A., Weinelt M., Schneider R., Mix A.C., Abelmann A.,
909 Armand L., Bard E., Barker S., Barrows T.T., Benway H., Cacho I., Chen M.T., Cortijo E., Crosta X., de
910 Vernal A., Dokken T., Duprat J., Elderfield H., Eynaud F., Gersonde R., Hayes A., Henry M., Hillaire-
911 Marcel C., Huang C.C., Jansen E., Juggins S., Kallel N., et al. 2009. Constraints on the magnitude and
912 patterns of ocean cooling at the Last Glacial Maximum. Nature Geoscience, 2(2): 127-132.

913 Zielinski U., Gersonde R., Sieger R. & Futterer D. 1998. Quaternary surface water temperature
914 estimations: Calibration of a diatom transfer function for the Southern Ocean. Paleoceanography,
915 13(4): 365-383.